REPORT

PLANETARY SCIENCE

Background levels of methane in Mars' atmosphere show strong seasonal variations

Christopher R. Webster[1]*, Paul R. Mahaffy[2], Sushil K. Atreya[3], John E. Moores[4], Gregory J. Flesch[1], Charles Malespin[2], Christopher P. McKay[5], German Martinez[3], Christina L. Smith[4], Javier Martin-Torres[6,7], Javier Gomez-Elvira[8], Maria-Paz Zorzano[6,8], Michael H. Wong[3], Melissa G. Trainer[2], Andrew Steele[9], Doug Archer Jr.[10], Brad Sutter[10], Patrice J. Coll[11], Caroline Freissinet[12], Pierre-Yves Meslin[13], Raina V. Gough[14], Christopher H. House[15], Alexander Pavlov[2], Jennifer L. Eigenbrode[2], Daniel P. Glavin[2], John C. Pearson[1], Didier Keymeulen[1], Lance E. Christensen[1], Susanne P. Schwenzer[16], Rafael Navarro-Gonzalez[17], Jorge Pla-García[8,18], Scot C. R. Rafkin[19], Álvaro Vicente-Retortillo[3], Henrik Kahanpää[20], Daniel Viudez-Moreiras[8], Michael D. Smith[2], Ari-Matti Harri[20], Maria Genzer[20], Donald M. Hassler[19], Mark Lemmon[21], Joy Crisp[1], Stanley P. Sander[1], Richard W. Zurek[1], Ashwin R. Vasavada[1]

Variable levels of methane in the martian atmosphere have eluded explanation partly because the measurements are not repeatable in time or location. We report in situ measurements at Gale crater made over a 5-year period by the Tunable Laser Spectrometer on the Curiosity rover. The background levels of methane have a mean value 0.41 ± 0.16 parts per billion by volume (ppbv) (95% confidence interval) and exhibit a strong, repeatable seasonal variation (0.24 to 0.65 ppbv). This variation is greater than that predicted from either ultraviolet degradation of impact-delivered organics on the surface or from the annual surface pressure cycle. The large seasonal variation in the background and occurrences of higher temporary spikes (~7 ppbv) are consistent with small localized sources of methane released from martian surface or subsurface reservoirs.

Methane is produced in Earth's atmosphere predominantly through biological processes (*1*, *2*). Its existence in an oxidizing atmosphere such as Mars' is recognized as a potential biosignature whose putative sources could include methanogenic bacteria (*1*, *3*, *4*). Alternative nonbiological methane production mechanisms include geological processes such as serpentinization of olivine or pyroxene (*5*), ultraviolet (UV) degradation of indigenous or meteoritically delivered organics (*6*, *7*), formation by the impact of comets (*8*), release from subsurface clathrates (*9*) or gas absorbed in the regolith (*10*, *11*), erosion of basalt with methane inclusions (*12*), or geothermal processes (*13*). As a strong greenhouse gas, methane bursts on early Mars may have been responsible for intermittent lake-forming climates—a process which could be ongoing today (*14*).

There have been numerous reports of methane in Mars' atmosphere by Earth-based remote sensing and from Mars orbit since 2004. None of those observations show a repeatable seasonal, temporal, or spatial trend. From Earth telescopes, a global average value of 10 ± 3 parts per billion by volume (ppbv) was observed in 1999 (*3*), whereas observations in 2003 showed plumes of methane from discrete sources with a summertime maximum of ~45 ppbv near the equator (*4*), but only an upper limit of 7.8 ppbv 3 years later in January 2006 (*15*). Further data taken in February 2006 yielded a detection of 10 ppbv at 45°S to 7°N over the Valles Marineris region, but an upper limit of 3 ppbv outside that region, and no detection (<8 ppbv) in December 2009 (*16*). From Mars orbit, the Planetary Fourier Spectrometer (PFS) on the Mars Express spacecraft measured a global average abundance of 15 ± 5 ppbv from 2004 to 2010 (*17*, *18*). The Thermal Emission Spectrometer on the Mars Global Surveyor spacecraft measured abundances ranging from 5 to 60 ppbv (*19*), although the claims of local variations were later withdrawn (*20*). Published maps of PFS data (*18*) at Curiosity's landing site in Gale crater (4.5°S, 137°E) show an increase over 1 year from ~15 ppbv in Autumn to ~30 ppbv in winter. In situ measurements of Mars methane began soon after the August 2012 landing of the Mars Science Laboratory (MSL) Curiosity rover at Gale crater. The Tunable Laser Spectrometer (TLS) of the Sample Analysis at Mars (SAM) instrument suite initially reported (*21*) a low methane abundance at Gale crater with an upper limit of 1.3 ppbv [95% confidence interval (CI)]. Subsequent observations over a 20-month period showed (*22*) a background level of 0.69 ± 0.25 ppbv and revealed unexpected occasional spikes to 7.2 ± 2.1 ppbv (95% CI).

Existing models including atmospheric transport and circulation (*23*–*26*) are unable to reproduce the reported high concentrations of methane and its spatial and temporal variability, even when including possible clathrate release (*9*), surface/regolith adsorption/desorption (*10*), seasonally variable production from UV breakdown of surface organics (*6*, *7*), or proposed mechanisms of rapid loss (*27*, *28*). Analysis of all methane measurements up to 2016 (*29*) provides little evidence for any correlation between meteor streams and methane plumes as previously suggested (*30*).

The TLS-SAM instrument (*31*) is a two-channel tunable laser spectrometer that uses both direct and second harmonic detection of absorbed infrared (IR) laser light. One channel uses a near-IR tunable diode laser at 2.78 μm to measure carbon, oxygen, and hydrogen isotopic ratios in both the Mars atmosphere and from gases evolved from rock pyrolysis (*32*, *33*). The high spectral resolution provides high sensitivity to methane by resolving its distinct fingerprint spectral pattern of three adjacent R(3) $^{12}CH_4$ lines in the 3.3-μm band (*32*). An interband cascade semiconductor laser source reflects 81 times between two spherical mirrors in a 20-cm-long sample cell of the Herriott design. The sample cell is fitted with high-vacuum microvalves to control evacuation by a SAM turbomolecular pump for empty cell scans or is filled to Mars

[1]NASA Jet Propulsion Laboratory, California Institute of Technology, Pasadena, CA, USA. [2]NASA Goddard Space Flight Center, Greenbelt, MD, USA. [3]Department of Climate and Space Sciences and Engineering, University of Michigan, Ann Arbor, MI, USA. [4]Department of Earth and Space Science and Engineering, York University, Toronto, ON, Canada. [5]NASA Ames Research Center, Moffett Field, CA, USA. [6]Department of Computer Science, Electrical and Space Engineering, Luleå University of Technology, Luleå, Sweden. [7]Instituto Andaluz de Ciencias de la Tierra, Granada, Spain. [8]Centro de Astrobiología, Instituto National de Tecnica Aerospacial, Madrid, Spain. [9]Geophysical Laboratory, Carnegie Institution for Science, Washington, DC, USA. [10]Jacobs Technology, NASA Johnson Space Center, Houston, TX, USA. [11]Laboratoire Interuniversitaire des Systèmes Atmosphériques, Creteil Cedex, France. [12]Laboratoire Atmosphères, Milieux, Observations Spatiales, Paris Cedex 05, France. [13]Institut de Recherche en Astrophysique et Planétologie, Toulouse, France. [14]Department of Chemistry and Biochemistry and Cooperative Institute for Research in Environmental Sciences, University of Colorado, Boulder, CO, USA. [15]Department of Geosciences, Pennsylvania State University, University Park, PA, USA. [16]School of Environment, Earth and Ecosystem Sciences, Open University, Milton Keynes, UK. [17]Instituto de Ciencias Nucleares, Universidad Nacional Autonoma de Mexico, Ciudad Universitaria, Mexico City, Mexico. [18]Space Science Institute, Boulder, CO, USA. [19]Department of Space Studies, Southwest Research Institute Boulder, Boulder, CO, USA. [20]Finnish Meteorological Institute, Helsinki, Finland. [21]Department of Atmospheric Sciences, Texas A&M University, College Station, TX, USA.
***Corresponding author. Email: chris.r.webster@jpl.nasa.gov**

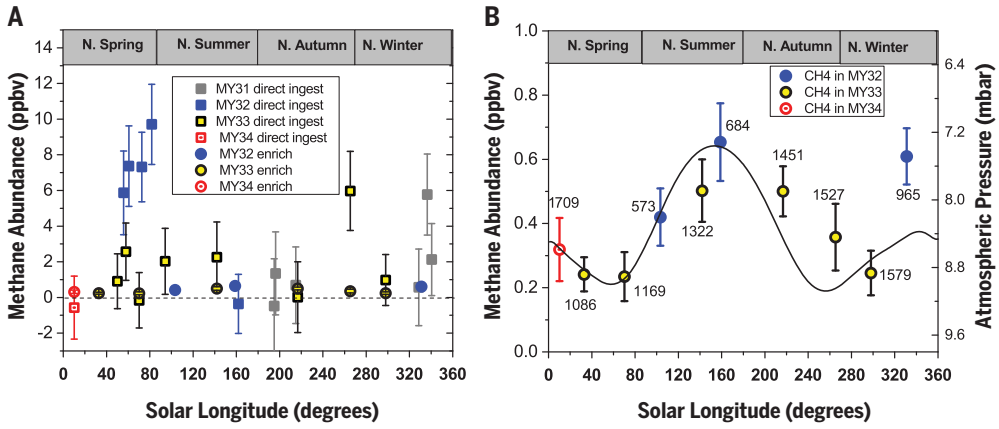

Fig. 1. The TLS-SAM methane measurements versus martian solar longitude. All plotted values are listed in table S2, have error bars of ± 1 SEM, and are corrected to global mean annual values. MY, Mars year. (**A**) All measurements up to 27 May 2017, including those from direct ingests (squares) and enrichment ingests (circles with smaller error bars). (**B**) Background measurements from enrichment ingests show strong seasonal variation. The atmospheric pressure (inverted scale at right) from REMS is plotted for comparison, the solid line representing the mean values over the 3 Mars years.

ambient pressure (~7 mbar) for full cell runs. Because the instrument's foreoptics chamber contains residual terrestrial methane gas, an atmospheric determination is made by subtracting an empty cell measurement from each full cell run (*34*). We used two methods of atmospheric ingestion: The first is a direct ingest method, in which gas is fed into the evacuated sample cell through an inlet port located on the side of the Curiosity rover, taking ~20 min to fill to ~7 mbar and producing uncertainties of ~2 ppbv for each measurement (*34*). The second is an enrichment method that ingests atmospheric gas through a second inlet port, which is passed over a CO_2 scrubber to fill the sample cell more slowly (~2 hours) to the same pressure of ~7 mbar. The latter method efficiently removes incoming CO_2 and H_2O but not methane, effectively enriching its abundance by a factor of 25 ± 4 (*34*). This reduces the overall uncertainty correspondingly, allowing more precise determination of low background levels. Along with other monitoring data, the Herriott cell pressure is recorded every 3 s during the entire ingestion process and data collection.

All our measurements to 27 May 2017 (values listed in table S2), over a period of 55 (Earth) months spanning 3 martian years, are shown in Fig. 1A. We consider values above 3 ppbv to be high spikes of methane; these were occasionally observed in the direct ingest mode. For the high methane spike seen in direct ingest on the four sols (martian days since rover landing) 467, 475, 505, and 525, our improved analysis (*34*) produces a mean value of 7.6 ± 1.6 ppbv (95% CI), which is slightly higher than the 7.2 ppbv previously reported (*22*). All high-precision measurements in the enrichment mode are below 0.7 ppbv and identify the background levels and their associated seasonal variation. These individual background level measurements are given in Table 1, with a mean value of 0.41 ± 0.16 (95% CI) and a variation that ranges from 0.24 to 0.65 ppbv, an increase of nearly a factor of 3 from its lowest value.

As shown in Fig. 1B, the background methane levels have a strong seasonal cycle, peaking near the end of the northern summer/southern winter (Gale crater at 4.5°S, 137.4°E is near the equator). There is no large variation in the mean background level from year to year over this period. The direct ingest measurements with values below 3 ppbv produce a mean value of 0.59 ± 0.54 (95% CI), which is consistent with the higher precision enrichment mean value. This rules out some potential contamination sources because direct ingest uses a different inlet and plumbing from the enrichment runs. Indeed, for the many occasions (table S2) when a direct ingest measurement was run soon after an enrichment run (~4 hours between sample midpoints), the two results agree within the uncertainty of the direct ingest measurement, with only one exception on sol 1527 [solar longitude (L_s) = 265.3°]. On this sol, a 20-min direct atmospheric ingest started 3 hours after the end of a 2-hour atmospheric enrichment ingest. The direct sample contained 5.98 ppbv CH_4, whereas the enriched sample contained 0.27 ppbv CH_4. We attribute this to the arrival at Curiosity of a high spike from a location that could have been up to tens of kilometers away, according to model wind fields (*34*). The enrichment value at L_s = 331° of 0.61 ppbv appears higher than expected for a single modal seasonal variation shape, so we cannot rule out that this may be due to the atmosphere in recovery from a higher spike sometime before that measurement.

An earlier report (*22*) ruled out several mechanisms that may have caused false TLS readings—namely, methane left over from evolved-gas pyrolysis of rock samples, incomplete pumping of the Herriott cell, reactive coatings inside the Herriott cell, wheel degradation or rock-crushing release during transit, and varying surface material under the rover. We argue against the possibility (*35*) that the rover itself is a source of methane because we cannot identify any source large enough to produce even an instantaneous cloud of ~7 ppbv methane in a 10-m-diameter sphere around the rover, which would require ~10^{18} methane molecules (*34*). With typical Mars wind speeds of ~3 to 5 m/s (*36*) replenishing the air around the rover, a supply of ~10^{24} methane molecules would be needed over the 2-month duration of the highest spike period. Although the TLS-SAM fore-optics chamber contains some terrestrial methane [~10^{15} molecules (*34*)], this is too small an amount to be considered as a bulk source for later ingestion even if somehow contained within the rover instrumentation. By monitoring the fore-optics chamber pressure and methane content over the 5-year period on Mars, we see no evidence of gross leakage from the foreoptics chamber.

Correlations of the high methane spikes with other measurements were investigated in an earlier publication (*22*). We compare our background values with the same parameters measured by Curiosity's instruments (*34*): pressure, surface temperature, relative humidity, inferred water vapor abundance, and surface UV from the Rover Environmental Monitoring Station (REMS) instrument; dust opacity from REMS and the Mastcam instrument; radiation flux from the Radiation Assessment Detector (RAD) instrument; and argon measurements from SAM's Quadrupole Mass Spectrometer (QMS).

The rough seasonal trend of a maximum near the end of northern summer is seen in several parameters—including the atmospheric pressure, surface UV, surface temperature, and argon abundance—but comparing these small seasonal changes with our methane background measurements produces no significant bivariate linear correlation (figs. S3 to S38) (*34*).

As with all Solar System bodies, Mars is expected to receive material exogenously (from outside the planet) as infalling dust, micrometeorites, and cometary sources containing organic materials that can partially survive (or be reexposed during atmospheric entry) on the surface, later releasing methane from UV photolytic processes either directly (*7*) or through secondary photochemical reaction (*37*). One such UV/CH_4 model (*7*) predicts that production is carbon-limited and over very long time periods can produce 2.2 ppbv methane in the martian atmosphere. We considered models of methane arising from exogenous material but found that they are inconsistent with the observed background value, its disproportionality with the UV flux, and the size of its seasonal variation (*34*).

The Mars atmosphere has a seasonal surface pressure cycle due to a combination of the

Table 1. Curiosity TLS-SAM methane enrichment measurements at Gale crater (4.5°S, 137.4°E) over a 38-month period. SEM, standard error of the mean; EF, enrichment factor; L_s, solar longitude; CI, confidence interval. The global pressure multiplier is derived from in situ REMS pressure measurements; it is the number by which the original measured in situ values of methane (given in table S3) were multiplied to correct the results to the global mean annual mixing ratio given in the right two columns. Earth dates refer to the time when the gas ingest was started. The decimal portion of the sol is used so that sol 573.08 represents local time 01:57.

Martian sol after landing on 6 August 2012	Earth date	L_s (degrees)	Global pressure multiplier	CH_4 (ppbv)	Error ± 1 SEM (ppbv)
573.08	17 March 2014	103.48	0.970	0.419	0.089
684.06	9 July 2014	158.61	0.877	0.653	0.121
965.99	25 April 2015	331.57	1.003	0.609	0.088
1086.06	26 August 2015	32.81	1.050	0.241	0.053
1169.02	19 November 2015	70.57	1.062	0.235	0.076
1322.00	24 April 2016	142.46	0.881	0.502	0.097
1451.06	4 September 2016	216.58	1.007	0.500	0.078
1527.06	21 November 2016	265.78	1.076	0.357	0.104
1579.00	13 January 2017	298.76	1.036	0.246	0.069
1709.00	27 May 2017	10.84	1.020	0.319	0.098
				Mean value ± 1 SEM (68% CI) = 0.408 ± 0.049 ppbv	
				Mean value including EF error ± 1 SEM (68% CI) = 0.408 ± 0.082 ppbv	
				Mean value ± 2 SEM (95% CI) = 0.41 ± 0.16 ppbv	

condensation and sublimation of carbon dioxide in the polar caps, an effect arising from the difference in mean surface altitude of the two hemispheres, and a dynamical effect resulting from the balance between mass and wind field (*38*). At equatorial locations like Gale crater, the pressure cycle is dominated by the polar cap contribution, although departures from regular seasonal trends can be present locally, sometimes because of dust storms (*39*). In situ measurements from REMS show pressures that range from 7.3 to 9.1 mbar (Fig. 1B), with a mean value of 8.4 mbar. When reporting gas mixing ratios, it is customary to correct in situ values to produce global mean annual mixing ratios, as we have done for the TLS-SAM data (Table 1 and Fig. 1). The observations of spatial and temporal variations (such as the spikes) indicate that normalization to a global mean value may not be appropriate, although this correction is at most only ~15% of the observed amplitude. To explain the large amplitude of the background methane observations, we considered whether large quantities of poorly mixed subliming CO_2 could reach the low latitudes of Gale crater during the higher pressures and thereby result in low mixing ratios locally; this scenario is not borne out by modeling (*36*) nor by the QMS-SAM in situ measurements of argon (*34*), which can be considered a long-lived tracer of atmospheric transport and mixing.

The Mars Regional Atmospheric Modeling System (MRAMS) (*34*) shows that both horizontal mixing and vertical transport play a role in the transport of air into and out of Gale crater. For a small (~2° latitude/longitude area) short (~1 hour) methane release inside Gale crater, all methane is gone (reduced by an order of magnitude) within 6 to 8 hours; when released outside the crater, methane is diluted by several orders of magnitude in similar time, regardless of the season. Mixing time scales are ~1 sol regardless of season, which is much faster than previously thought (*34*). For steady-state release in a small to medium area (~2° to 10° latitude/longitude area) mimicking expectations for release inside or outside the crater, MRAMS shows daily variations of an order of magnitude occurring because of nighttime/daytime differences in flows between crater rim and floor.

With ancient atmospheric pressures of several hundred millibars (*40*), large amounts of methane may be stored in the cold martian subsurface as clathrates in a stability zone several times thicker than that of Earth (*41*–*43*). Although the seasonal signature of the TLS-SAM measurements is not consistent with direct clathrate release, clathrates may provide a source of surface microseepage (diffuse exhalations without any specific morphological structure that may vent from outcropping of rocks or river or lake beds) (*43*–*45*). On Mars, such seepage would occur preferentially through permeable pathways, such as faults, fractures, or in breaches in sealing lithologies; this would not require identifiable geomorphological structures on the surface. Weak microseepage exhalations could explain background and plume methane anomalies observed on Mars (*43*), perhaps near the dichotomy boundary and at Gale crater, where there is fractured sedimentary rock. Microseepage flux may vary over time, depending on variations of gas pressures along the subsurface migration pathway or on seasonal changes in the soil, or even where microbial activity may consume methane.

Regardless of the subsurface origin, methane that finds its way to surface layers over long time periods (*42*, *43*) may be expected to show seasonal variation. We consider a process that retains methane at the surface temporarily before releasing it through a process linked to the surface temperature. That process could be adsorption on a surface with a high surface area–to-volume ratio, such as dust or soil. Although mineral dust cannot serve as a methane sink, it can moderate the release (*11*, *12*). Adopting an energy barrier of ~20 to 35 kJ/mol—which is somewhat higher than that reported for the physical adsorption of methane into clays (*46*), zeolites (*47*), and Mars analog soil (*12*)—we found that large seasonal variations are expected (fig. S41). Plausible correlations of the background methane values with atmospheric water vapor and with surface temperatures point to physical or chemical surface (or dust) processes, or microseepage release. The amplitude of the seasonal cycle indicates that there remain unknown atmospheric or surface processes occurring in present-day Mars.

REFERENCES AND NOTES

1. S. K. Atreya, P. R. Mahaffy, A. S. Wong, *Planet. Space Sci.* **55**, 358–369 (2007).
2. Core Writing Team, Intergovernmental Panel for Climate Change (IPCC), *Fifth Assessment Report 2014*, R. K. Pachauri, L. A. Meyer, Eds. (IPCC, 2014); www.ipcc.ch.
3. V. A. Krasnopolsky, J. P. Maillard, T. C. Owen, *Icarus* **172**, 537–547 (2004).
4. M. J. Mumma *et al*., *Science* **323**, 1041–1045 (2009).
5. C. Oze, M. Sharma, *Geophys. Res. Lett.* **32**, L10203 (2005).
6. F. Keppler *et al*., *Nature* **486**, 93–96 (2012).
7. A. Schuerger, J. E. Moores, C. A. Clausen, N. G. Barlow, D. T. Britt, *J. Geophys. Res.* **117**, E08007 (2012).
8. V. A. Krasnopolsky, *Icarus* **180**, 359–367 (2006).
9. E. Chassefière, *Icarus* **204**, 137–144 (2009).
10. P.-Y. Meslin, R. Gough, L. Lefevre, F. Forget, *Planet. Space Sci.* **59**, 247–258 (2010).
11. R. V. Gough, M. A. Tolbert, C. P. McKay, O. B. Toon, *Icarus* **207**, 165–174 (2010).
12. S. McMahon, J. Parnell, N. J. F. Blamey, *Int. J. Astrobiol.* **12**, 113–122 (2013).
13. G. Etiope, D. Z. Oehler, C. C. Allen, *Planet. Space Sci.* **59**, 182–195 (2011).
14. E. S. Kite *et al*., *Nat. Geosci.* **10**, 737–740 (2017).
15. G. L. Villanueva *et al*., *Icarus* **223**, 11–27 (2013).
16. V. A. Krasnopolsky, *Icarus* **217**, 144–152 (2012).
17. V. Formisano, S. Atreya, T. Encrenaz, N. Ignatiev, M. Giuranna, *Science* **306**, 1758–1761 (2004).

18. A. Geminale, V. Formisano, G. Sindoni, *Planet. Space Sci.* **59**, 137–148 (2011).
19. S. Fonti, G. A. Marzo, *Astron. Astrophys.* **512**, A51 (2010).
20. S. Fonti *et al.*, *Astron. Astrophys.* **581**, A136 (2015).
21. C. R. Webster, P. R. Mahaffy, S. K. Atreya, G. J. Flesch, K. A. Farley, MSL Science Team, *Science* **342**, 355–357 (2013).
22. C. R. Webster *et al.*, *Science* **347**, 415–417 (2015).
23. F. Lefèvre, F. Forget, *Nature* **460**, 720–723 (2009).
24. S. K. Atreya *et al.*, *Planet. Space Sci.* **59**, 133–136 (2011).
25. K. J. Zahnle, R. S. Freedman, D. C. Catling, *Icarus* **212**, 493–503 (2011).
26. M. A. Mischna, M. Allen, M. I. Richardson, C. E. Newman, A. D. Toigo, *Planet. Space Sci.* **59**, 227–237 (2011).
27. S. K. Atreya *et al.*, *Astrobiology* **6**, 439–450 (2006).
28. W. M. Farrell, G. T. Delory, S. K. Atreya, *J. Geophys. Res.* **33**, L21203 (2006).
29. M. Roos-Serote, S. K. Atreya, C. R. Webster, P. R. Mahaffy, *J. Geophys. Res.* **121**, 2108–2119 (2016).
30. M. Fries *et al.*, *Geochem. Perspect. Lett.* **2**, 10–23 (2016).
31. P. R. Mahaffy *et al.*, *Space Sci. Rev.* **170**, 401–478 (2012).
32. C. R. Webster, P. R. Mahaffy, *Planet. Space Sci.* **59**, 271–283 (2011).
33. C. R. Webster *et al.*, *Science* **341**, 260–263 (2013).
34. Materials and methods are available as supplementary materials.
35. K. Zahnle, *Science* **347**, 370–371 (2015).
36. C. E. Newman *et al.*, *Icarus* **291**, 203–231 (2017).
37. J. R. C. Garry, I. L. ten Kate, Z. Martins, P. Nørnberg, P. Ehrenfreund, *Meteorit. Planet. Sci.* **41**, 391–405 (2006).
38. F. Hourdin, P. Le Van, F. Forget, O. Talagrand, *J. Atmos. Sci.* **50**, 3625–3640 (1993).
39. G. M. Martínez *et al.*, *Space Sci. Rev.* **212**, 295–338 (2017).
40. B. M. Jakosky, R. J. Phillips, *Nature* **412**, 237–244 (2001).
41. B. K. Chastain, V. Chevrier, *Planet. Space Sci.* **55**, 1246–1256 (2007).
42. O. Mousis *et al.*, *Icarus* **278**, 1–6 (2016).
43. D. Z. Oehler, G. Etiope, *Astrobiology* **17**, 1233–1264 (2017).
44. G. Etiope, *Natural Gas Seepage: The Earth's Hydrocarbon Degassing* (Springer, 2015).
45. M. G. Trainer, M. A. Tolbert, C. P. McKay, O. B. Toon, *Icarus* **208**, 192–197 (2010).
46. P. R. Pereira, J. Pires, M. Brotas de Carvalho, *Separ. Purif. Tech.* **21**, 237–246 (2001).
47. S. Y. Zhang, O. Talu, D. T. Hayhurst, *J. Phys. Chem.* **95**, 1722–1726 (1991).

ACKNOWLEDGMENTS

The authors thank the reviewers for constructive comments that greatly improved the manuscript. The research described here was carried out in part at the Jet Propulsion Laboratory, California Institute of Technology, under a contract with the National Aeronautics and Space Administration (NASA). **Funding:** Funding from NASA's Planetary Science Division is acknowledged by authors C.R.W., P.R.M., S.K.A., G.J.F., C.M., C.P.M., M.H.W., M.G.T., A.S., D.A., C.H.H., R.V.G., A.P., J.L.E., D.P.G., J.C.P., D.K., L.E.C., J.P.-G., S.C.R.R., M.D.S., D.M.H., M.L., J.C., R.W.Z., and A.R.V. R.N.-G. acknowledges funding from the National Autonomous University of Mexico and Consejo Nacional de Ciencia y Tecnología. J.E.M. and C.L.S. acknowledge funding from the Canadian Space Agency MSL participating scientist program. S.P.Sc. acknowledges funding from the UK Space Agency. A.-M.H. acknowledges funding from the Finnish Academy under grant 310509. J.P.-G. acknowledges funding from the Spanish Ministry of Economy and Competitiveness under contract ESP2016-79612-C3-1-R. **Author contributions:** C.R.W. and P.R.M. performed TLS-SAM instrument design, build, and testing (IDBT); surface operations (SO); test-bed activities (TBA); data analysis (DA); data correlations (DC); and science interpretation (SI). G.J.F. and C.M. performed IDBT, SO, TBA, and DA. S.K.A., J.E.M., C.P.M., C.L.S., A.S., D.A., B.S., P.J.C., C.F., P.-Y.M., R.V.G., C.H.H., A.P., J.L.E., D.P.G., S.P.Sa., and R.W.Z. performed SI. J.C. and A.R.V. performed SO. J.C.P., D.K., and L.E.C. performed IDBT. G.M., J.M.-T., J.G.-E., M.-P.Z., M.G.T., S.P.Sc., R.N.-G., A.V.-R., H.K., D.V.-M., M.D.S., A.-M.H., M.G., D.M.H., and M.L. performed DC. J.P.-G. and S.C.R.R. performed DC and SI. **Competing interests:** No potential conflicts of interest exist for any of the listed authors. **Data and materials availability:** The data described in this paper are publicly available from NASA's Planetary Data System (PDS) under an arrangement with the Mars Science Laboratory (MSL) project at http://pds-geosciences.wustl.edu/missions/msl/sam.htm, under the run numbers given in table S2.

SUPPLEMENTARY MATERIALS

www.sciencemag.org/content/360/6393/1093/suppl/DC1
Materials and Methods
Supplementary Text
Figs. S1 to S44
Tables S1 and S2
References (*48*–*62*)

20 September 2017; accepted 4 May 2018
10.1126/science.aaq0131

Science

Background levels of methane in Mars' atmosphere show strong seasonal variations

Christopher R. Webster, Paul R. Mahaffy, Sushil K. Atreya, John E. Moores, Gregory J. Flesch, Charles Malespin, Christopher P. McKay, German Martinez, Christina L. Smith, Javier Martin-Torres, Javier Gomez-Elvira, Maria-Paz Zorzano, Michael H. Wong, Melissa G. Trainer, Andrew Steele, Doug Archer Jr., Brad Sutter, Patrice J. Coll, Caroline Freissinet, Pierre-Yves Meslin, Raina V. Gough, Christopher H. House, Alexander Pavlov, Jennifer L. Eigenbrode, Daniel P. Glavin, John C. Pearson, Didier Keymeulen, Lance E. Christensen, Susanne P. Schwenzer, Rafael Navarro-Gonzalez, Jorge Pla-García, Scot C. R. Rafkin, Álvaro Vicente-Retortillo, Henrik Kahanpää, Daniel Viudez-Moreiras, Michael D. Smith, Ari-Matti Harri, Maria Genzer, Donald M. Hassler, Mark Lemmon, Joy Crisp, Stanley P. Sander, Richard W. Zurek and Ashwin R. Vasavada

Science **360** (6393), 1093-1096.
DOI: 10.1126/science.aaq0131

Measuring martian organics and methane

The Curiosity rover has been sampling on Mars for the past 5 years (see the Perspective by ten Kate). Eigenbrode *et al.* used two instruments in the SAM (Sample Analysis at Mars) suite to catch traces of complex organics preserved in 3-billion-year-old sediments. Heating the sediments released an array of organics and volatiles reminiscent of organic-rich sedimentary rock found on Earth. Most methane on Earth is produced by biological sources, but numerous abiotic processes have been proposed to explain martian methane. Webster *et al.* report atmospheric measurements of methane covering 3 martian years and found that the background level varies with the local seasons. The seasonal variation provides an important clue for determining the origin of martian methane.

Science, this issue p. 1096, p. 1093; see also p. 1068

www.sciencemag.org/content/360/6393/1093/suppl/DC1

Supplementary Material for

Background levels of methane in Mars' atmosphere show strong seasonal variations

Christopher R. Webster,* Paul R. Mahaffy, Sushil K. Atreya, John E. Moores, Gregory J. Flesch, Charles Malespin, Christopher P. McKay, German Martinez, Christina L. Smith, Javier Martin-Torres, Javier Gomez-Elvira, Maria-Paz Zorzano, Michael H. Wong, Melissa G. Trainer, Andrew Steele, Doug Archer Jr., Brad Sutter, Patrice J. Coll, Caroline Freissinet, Pierre-Yves Meslin, Raina V. Gough, Christopher H. House, Alexander Pavlov, Jennifer L. Eigenbrode, Daniel P. Glavin, John C. Pearson, Didier Keymeulen, Lance E. Christensen, Susanne P. Schwenzer, Rafael Navarro-Gonzalez, Jorge Pla-García, Scot C. R. Rafkin, Álvaro Vicente-Retortillo, Henrik Kahanpää, Daniel Viudez-Moreiras, Michael D. Smith, Ari-Matti Harri, Maria Genzer, Donald M. Hassler, Mark Lemmon, Joy Crisp, Stanley P. Sander, Richard W. Zurek, Ashwin R. Vasavada

*Corresponding author. E-mail: chris.r.webster@jpl.nasa.gov

Published 8 June 2018, *Science* **360**, 1093 (2017)
DOI: 10.1126/science.aaq0131

This PDF file includes:

MATERIALS and METHODS:

Our method builds upon previously published material *(21, 22)* that is here updated and extended. We include updated results tables and correlation plots of the background methane measurements with a variety of observed quantities from MSL's SAM, REMS, RAD and Mastcam instruments, including pressure, relative humidity, water abundance, ground and surface air temperatures, UV insolation and atmospheric opacity.

The Tunable Laser Spectrometer (TLS) in the Sample Analysis at Mars (SAM) instrument suite on the Curiosity Rover has been described in detail *(22)*. This earlier material includes optical layout, photograph of the flight instrument, identification of the 3 spectral lines at 3057.7 cm^{-1} used for detection, spectral performance of the instrument, spectral data processing for both direct absorption and second harmonic detection, instrument calibration, a description of the empty cell-full cell-empty cell difference technique for producing sample cell methane abundances, and a detailed description of the methane enrichment method.

The main focus of this paper is on the background methane values produced from our methane enrichment runs, and so we summarize below the details of this method.

The methane enrichment process relies on the removal of CO_2 from the Mars atmosphere as it is ingested over a two-hour period across a CO_2 scrubber chamber that contains Linde 13X molecular sieve material. During the enrichment process, atmospheric gas is ingested through a second inlet port, and then passed over the CO_2 scrubber to more slowly fill the sample cell (~2 hours) to ~7 mbar. This efficiently removes the incoming CO_2 and H_2O but not methane, thereby effectively enriching the methane abundance. The enrichment factor (EF) is determined using a SAM test-bed at NASA GSFC (duplicate flight instruments, configurations, and code sequences to run various experiments, and including the flight-spare CO_2 scrubber with identical sieve material and volume). This determination was made sometime after the Curiosity landing, and no pre-launch comparisons were made, but we are confident that measurements performed on the SAM test-bed are representative of the flight instrument on Mars.

An earlier publication *(22)* reported only two measurements of Mars methane using the enrichment process, in which an enrichment factor EF of 23 ±1 was derived from 3 test-bed results on an identical (flight duplicate) scrubber with the same timing as that used on Mars. Since then, we have repeated our measured EF and added a measurement at a lower driving pressure of 5 mbar. The results are given below in Table S1. Although the mean value of the 4 measurements is 25.04 ±0.56, we recognize that the spread of values shows a potential increase with run sequence and a wide spread in values. In order to avoid underestimating the EF error, we increase this error by a factor of 4 to establish the systematic error associated with the enrichment factor of 25 ±2.2 (1sem), or 25 ±4.4 (2sem). The methane measurements presented in Table 1 show a random error given by the mean value of 0.408 ±0.049 ppbv, so combining this error with our EF systematic error produces a mean value of 0.408 ±0.082 ppbv (1sem), or 0.41 ±0.16 (2sem, or 95% CI).

Table S1. Enrichment Factors (EF) derived from SAM Test Bed experiments using supply (driving) pressures of 5-10 mbar. TID refers to "Test Identity" number used by SAM.

	TID	Driving Pressure		
2		mbar	EF	Error 1sem
3	52345	10	**21.05**	1.21
4	52351	10	**24.52**	1.13
5	52438	10	**26.5**	1.34
6	53054	5	**27.65**	0.65

The enrichment runs ingest the Martian atmosphere through a different inlet to that used for the direct-ingest runs *(22)*. Our first four methane measurements from the enrichment process (Sols 583, 684, 965, 1086) followed the empty cell/full cell/empty cell protocol described earlier *(22)*. Rather than continue either enrichment or direct-ingest runs on separate occasions, we developed a "hybrid" run script that recorded direct-ingest values immediately after the enrichment empty cell values. This "hybrid" run script was used for all subsequent sols, namely sols 1169, 1322, 1451, 1527, 1579, and 1709, and is graphically illustrated in Fig. S1 below. The "hybrid" script is a cut-and-paste copy of the individual enrichment and direct-ingest scripts, and so all enrichment values result from the identical enrichment script and procedure.

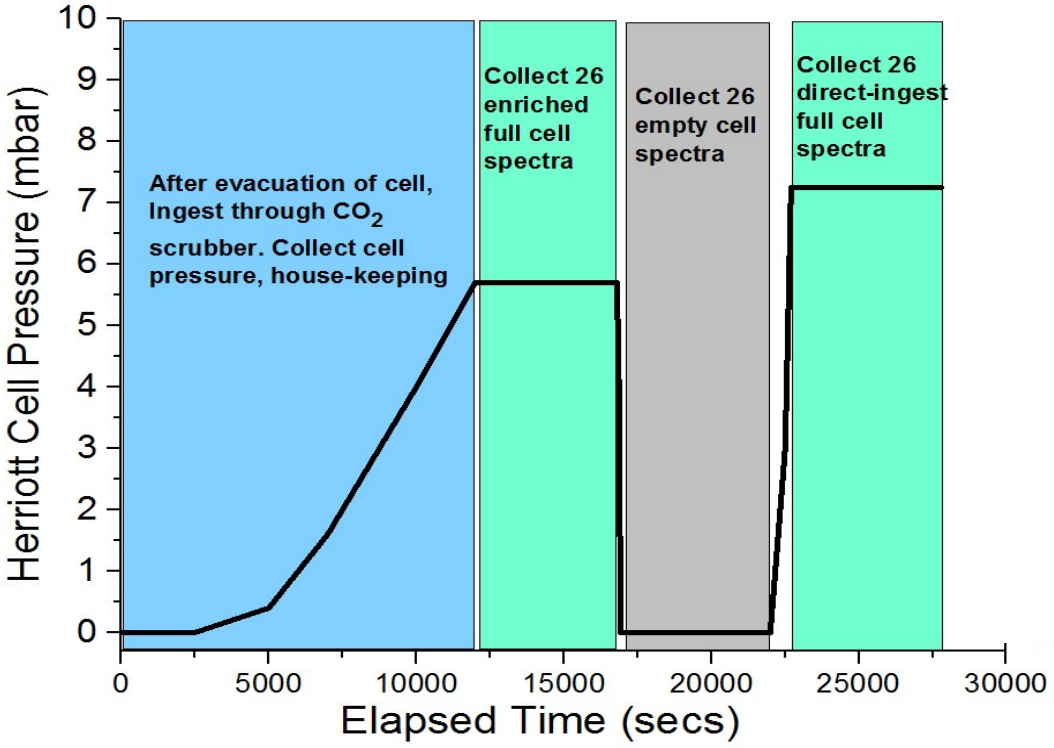

Fig. S1. The TLS-SAM hybrid enrichment run sequence produces both enriched values and subsequent direct-ingest values. This plot is based on actual pressure readings from the run of Sol 1451. Throughout the entire run, monitoring data (including Herriott cell and foreoptics pressures and temperatures) are recorded every 3 secs. The difference method is used to retrieve methane mixing ratios for enrichment and direct-ingest using the same empty cell values.

Curiosity's 5 years on Mars

Since landing at Yellowknife Bay in Gale crater on 6 August 2012, the Mars Science Laboratory (MSL) Curiosity Rover has traveled a total of ~20 km to end of December 2017 *(48)*, pausing to take numerous atmospheric gas samples and to drill rocks for sample analysis using the SAM and other instrument suites.

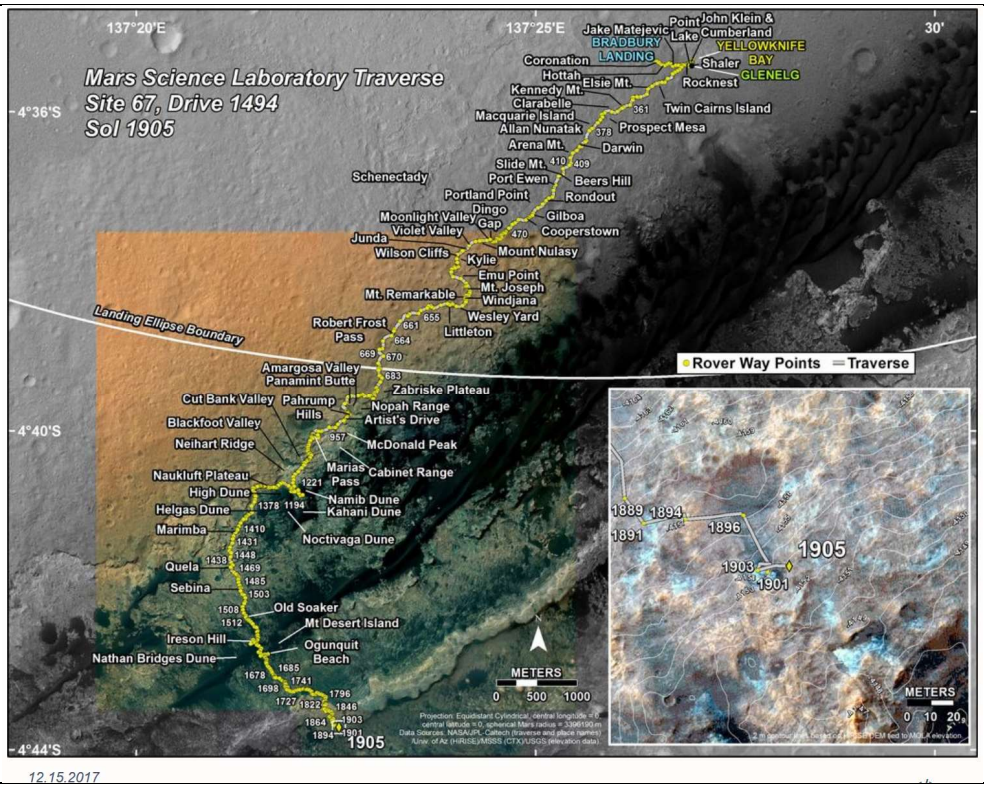

Fig. S2. The Curiosity Rover's path over the course of the mission up to December 12th 2017. See reference *(48)*. Courtesy NASA-JPL, publicly-available *(49)*.

The TLS-SAM Methane Data

Table S2 below provides all TLS-SAM measurements of methane to 27 May 2017 in chronological order.

Table S2. All data collected up to 27 May 2017, showing how in situ measurements are corrected to global annual mean mixing ratios through a global pressure multiplier based on REMS pressure measurements. As with Table 1 in the main text, temporal values (Sol, Ls, and Earth Date in Table 1) correspond to the start (valve open event) of each atmospheric ingest. The decimal portion of the sol is used such that e.g. sol 400.5 would represent local noon, and 400.75 would represent 1800 hours local time. Sol and Ls values for experiments #25103 and #25171 actually correspond to ingest sequences that were run as separate experiments, since these two "daytime" measurements were ingested and stored in the Herriott cell until the following night when SAM was able to run.

Run Type	Run #	Sol	Ls (deg)	In Situ CH_4 (ppbv)	Error (1SEM)	Global pressure multiplier Fp	Global mean CH_4 (ppbv)	Error (1SEM)
Direct-ingest	25028	79.96	195.60	-0.51	2.83	0.9381	-0.48	2.65
Direct-ingest	25029	81.89	196.77	1.43	2.47	0.942	1.35	2.33
Direct-ingest	25045	106.14	211.74	0.69	2.15	1.001	0.69	2.15
Direct-ingest	25096	293.16	329.16	0.56	2.14	1.009	0.57	2.16
Direct-ingest	25103	305.58	336.12	5.78	2.27	0.999	5.77	2.27
Direct-ingest	25104	314.14	340.83	2.13	2.03	0.997	2.13	2.02
Direct-ingest	25164	467.14	55.59	5.48	2.19	1.0706	5.87	2.35
Direct-ingest	25166	475.14	59.20	6.88	2.11	1.0706	7.37	2.26
Direct-ingest	25168	505.12	72.66	6.91	1.84	1.058	7.31	1.95
Direct-ingest	25171	525.56	81.84	9.34	2.16	1.039	9.71	2.25
Enrichment	25177	573.08	103.48	0.432	0.092	0.97	0.419	0.089
Enrichment	25206	684.06	158.61	0.745	0.138	0.877	0.653	0.121
Direct-ingest	25206	684.27	158.73	-0.41	1.89	0.879	-0.36	1.66
Enrichment	25266	965.99	331.57	0.607	0.087	1.0032	0.609	0.088
Enrichment	25284	1086.06	32.81	0.230	0.051	1.0503	0.241	0.053
Direct-ingest	25292	1125.14	50.81	0.85	1.44	1.0678	0.91	1.54
Direct-ingest	25299	1141.10	58.03	2.40	1.50	1.0709	2.57	1.61
Enrichment	25311	1169.02	70.57	0.221	0.072	1.063	0.235	0.076
Direct-ingest	25311	1169.23	70.66	-0.15	1.46	1.063	-0.16	1.55
Direct-ingest	25322	1222.10	94.50	2.03	1.85	1.002	2.03	1.85
Enrichment	25344	1322.00	142.46	0.570	0.110	0.8808	0.502	0.097
Direct-ingest	25344	1322.21	142.57	2.57	2.24	0.8808	2.26	1.97
Enrichment	25368	1451.06	216.58	0.497	0.077	1.0074	0.500	0.078
Direct-ingest	25368	1451.27	216.71	0.019	1.97	1.0074	0.019	1.98
Enrichment	25383	1527.06	265.78	0.332	0.097	1.0767	0.357	0.104
Direct-ingest	25383	1527.27	265.91	5.55	2.06	1.0767	5.97	2.22
Enrichment	25390	1579.00	298.76	0.237	0.067	1.0361	0.246	0.069
Direct-ingest	25390	1579.21	298.89	0.948	1.38	1.0361	0.982	1.43
Enrichment	25408	1709.00	10.84	0.313	0.097	1.0197	0.319	0.098
Direct-ingest	25408	1709.22	10.95	-0.56	1.73	1.0197	-0.57	1.76

Curiosity Instruments Providing Data for Comparison with TLS-SAM Methane:

The Rover Environmental Monitoring Station (REMS) *(50)* aboard the Curiosity rover consists of wind speed and direction, atmospheric and ground temperature, and atmospheric relative humidity sensors at 1.6 m height on the rover mast and pressure and UV sensors at 1 m height on the rover deck *(50)*. The Mast Camera (Mastcam) instrument aboard the Curiosity rover, mounted on the rover's remote sensing mast, takes direct images of the Sun at the wavelengths of 440 and 880 nm from which the atmospheric dust opacity can be retrieved *(51-53)*.

The REMS nominal strategy for data acquisition consists of 5 min-long hourly samples at 1 Hz throughout the mission, with interspersed full hour sample periods at 1 Hz to cover every time of the sol over a period of a few sols, while the Mastcam nominal strategy for atmospheric opacity retrievals consists of measurements made every three to seven sols.

We analyze the complete set of REMS and Mastcam observations and provide values of the daily mean atmospheric surface pressure, daily mean, maximum and minimum ground temperature, daily mean air temperature, daily maximum relative humidity, daily most-reliable water vapor volume mixing ratio, atmospheric opacity at 880 nm, and daily UV insolation (defined as the total amount of solar energy received during 1 sol from the UV region of the spectrum) at the surface and at the top of the atmosphere.

To calculate representative values of daily mean atmospheric surface pressure, atmospheric temperature and ground temperature, we only use measurements taken on sols that have full diurnal coverage. To calculate the daily maximum and minimum ground temperature, we also consider measurements on sols without full diurnal coverage but with high-confidence measurements (power supply in its operation range, the highest recalibration quality and with no shadows in the field of view) during the times when the ground temperature typically shows the daily maximum (between 12:00 and 14:00) and minimum (between 04:00 and 06:00) values. To calculate the daily maximum relative humidity (usually occurring between 04:00 and 06:00 local mean standard time), we only consider relative humidity measurements taken during the first four seconds after the sensor has been turned on after at least ~5 min of inactivity. After four seconds, relative humidity measurements spuriously decrease due to effects of heating. Reliable values include relative humidity measurements taken during the nominal and high-resolution interval mode, which consists of alternately switching the sensor on and off at periodic intervals to minimize heating and is only used on selected one to two hour observation blocks *(50)*. To calculate the daily most-reliable water vapor volume mixing ratio, we use the daily maximum relative humidity and simultaneous measurements of air temperature and pressure. Daytime REMS-derived volume mixing ratio values present large uncertainties due to the extremely low values of relative humidity and therefore cannot be obtained reliably *(50)*.

The REMS UV sensor is located on the rover deck and is composed of six photodiodes in the following ranges: 315-370 nm (UVA), 280-320 nm (UVB), 220-280 nm (UVC), 200-370 nm (total dose), 230-290 nm (UVD), and 300-350 nm (UVE), with an accuracy better than 8% of the full range for each channel, computed based on Mars radiation levels and minimum dust opacity. The photodiodes face the zenith direction and have a field of view of 60 degrees. To calculate the daily UV insolation at the surface, we use the photodiode output currents of the REMS UVE channel (300-350 nm), the ancillary data records containing the geometry of the rover and the Sun, the values of the atmospheric opacity at the reference wavelength of 880 nm, a Monte Carlo radiative transfer scheme and the Comimart radiative transfer model *(51)* following the procedure described in Vicente-Retortillo et al. *(53)*. Degradation of the UV sensor with dust accumulation is described in *(53)*.

The Radiation Assessment Detector (RAD) *(54)* on board the Curiosity rover measures the radiation environment at the surface of Gale crater on Mars *(55)*. Specifically, RAD measures spectra of charged particles with energies of a few tens up to a few hundred MeV per nucleon

(56) and neutral particle spectra between about 10 MeV and a few hundred MeV *(57)*. This surface radiation field mainly consists of primary Galactic Cosmic Rays (GCRs) and secondary, charged and neutral particles created by interactions of GCRs with the nuclei of the Martian atmosphere and soil *(56, 57)*. The intensity of this surface radiation field varies with atmospheric column depth above the rover location as well as heliospheric modulation as a function of the solar cycle.

Correlations of Background Methane Measurements with Other Measurements From Curiosity

This section presents individual plots showing the correlations between TLS enrichment measurements of CH_4 and environmental variables. Each page focuses on a single environmental variable. On each page, the first two plots show the exact same data arranged in two ways: first in chronological sequence, and then in overlapping martian years. The third plot of each page shows best linear fits to the CH_4 measurements as a function of the individual environmental variable.

Linear correlations are calculated for each environmental variable. We used methods based upon the "fit" and "gammq" routines from *(60)*, as implemented in the LINFIT IDL routine. The χ_ν^2 goodness-of-fit statistic is given for each correlation, and is based on the uncertainties in the TLS data given in Table S3 above. For a perfect linear fit, $\chi_\nu^2 = 1$. None of our tests give χ_ν^2 values close to 1. This indicates that it is unlikely that there is a simple linear relationship between any single environmental variable and the methane variation. Each plot also shows the probability that the fit would have a value of χ_ν^2 or greater. A believable linear relationship should have a probability of 0.1 or higher.

Data points on the third plot on each page (linear correlations) will have large horizontal error bars in cases where the environmental data are highly scattered rather than smoothly varying. This is because the horizontal error bars simply indicate the full range in the environmental variable, within 1° of L_S of the CH_4 measurement. For example, top of atmosphere (TOA) UV insolation and max. pressure are very smooth functions of time, so horizontal error bars in Figures S8 and S17 are very small. On the other hand, minimum ground temperatures within 1° of L_S of Sol 1709 (Fig. S22) had a large amount of scatter, producing a horizontal error bar in Fig. S23 of > 10 K. But for Sol 1527, Fig. S21 shows that min. ground temperatures were clustered tightly near 198 K. As a result, the horizontal error bar for Sol 1527 in Fig. S23 is < 2 K. These horizontal error bars are visual aids; only CH_4 measurement errors (y-error bars) were used in the linear fits (and related statistics) shown in the third plot of each page.

Correlation with surface UV insolation

Surface UV insolation is the solar energy incident at the surface integrated over the entire sol. The primary motivation for testing this variable is that solar UV may degrade organic material near the surface, releasing methane. Values come from a model described in *(53)*, and use empirical atmospheric dust loading estimates derived from Mastcam dust opacity imaging experiments and REMS UV-sensor measurements *(52, 53)*.

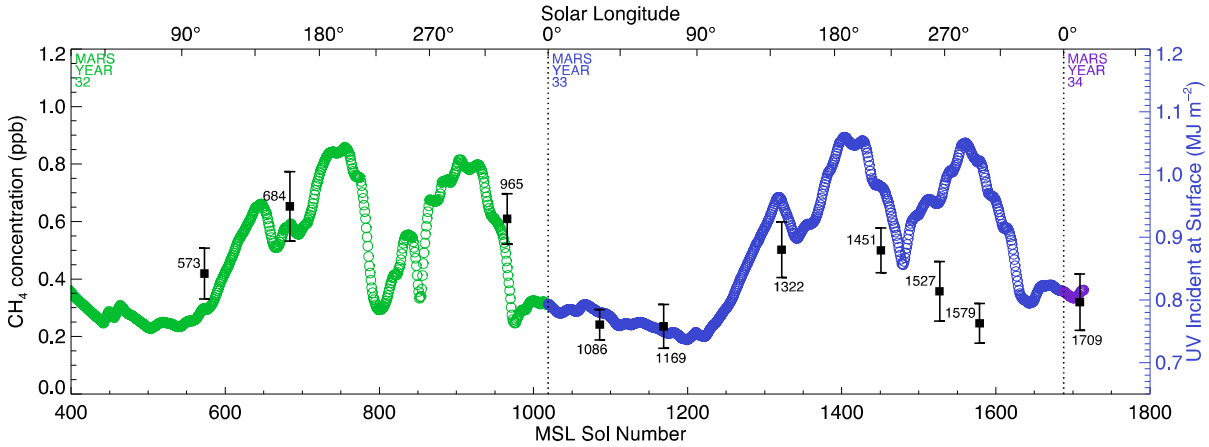

Fig. S3. CH_4 enrichment measurements (black squares with sol numbers) compared with UV surface insolation (colored circles) as a function of MSL mission sol number. Symbol color (and vertical lines) delineate Mars years.

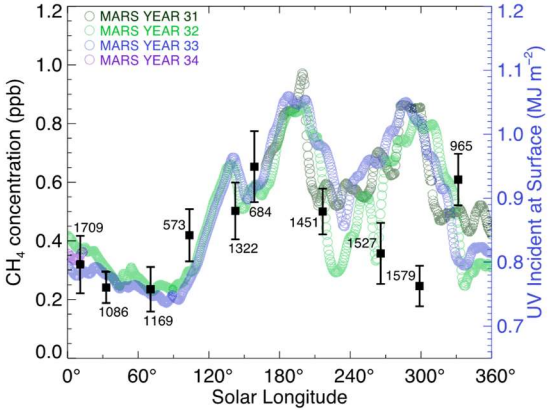

Fig. S4. CH_4 enrichment measurements (black squares with sol numbers) compared with UV surface insolation (colored circles) as a function of solar longitude (L_S). Symbol color denotes Mars year, as shown in upper left.

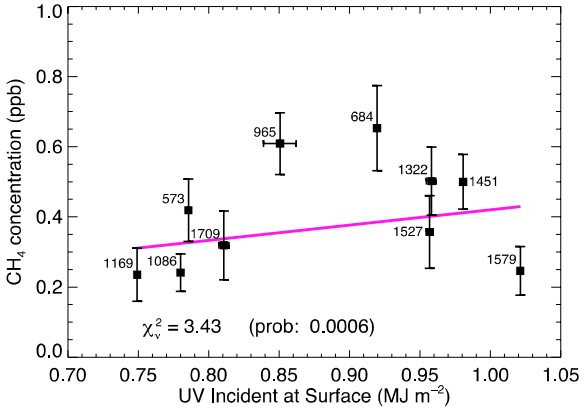

Fig. S5. Pink line shows best-fit linear correlation between CH_4 enrichment measurements (black squares with sol numbers) and UV surface insolation. The high χ_ν^2 and probability << 0.1 mean it is not likely there is a simple linear relationship between atmospheric CH_4 concentration and surface UV insolation.

Correlation with UV insolation at the top of the atmosphere

Top-of-atmosphere (TOA) UV insolation is the solar energy incident at Mars (at the latitude of Gale Crater) integrated over the entire sol. The motivation for testing this variable is that if organics are present in airborne dust, periods of high TOA UV insolation could generate more methane. TOA UV values are calculated analytically, as described in Vicente-Retortillo et al. *(53)*.

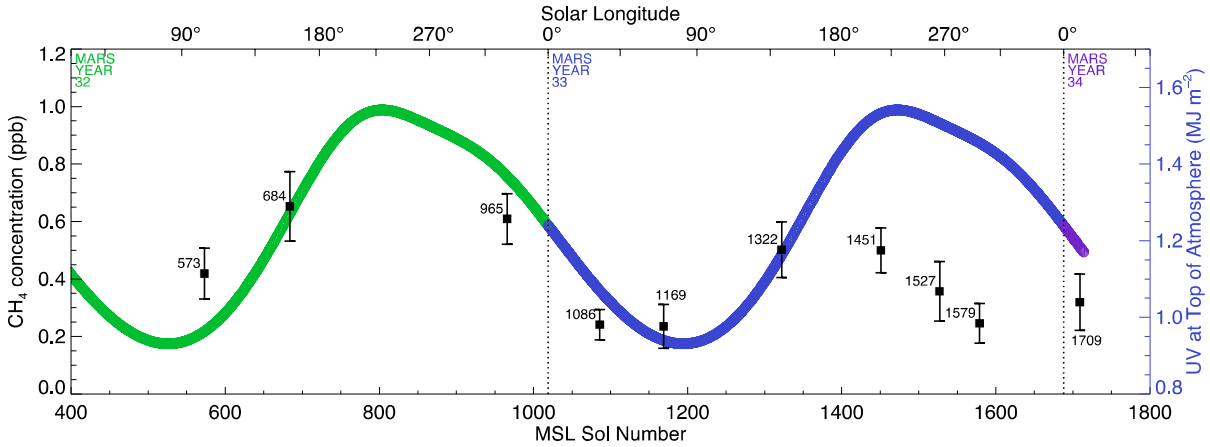

Fig. S6. As Fig. S3, but compared with UV top-of-atmosphere insolation (colored circles).

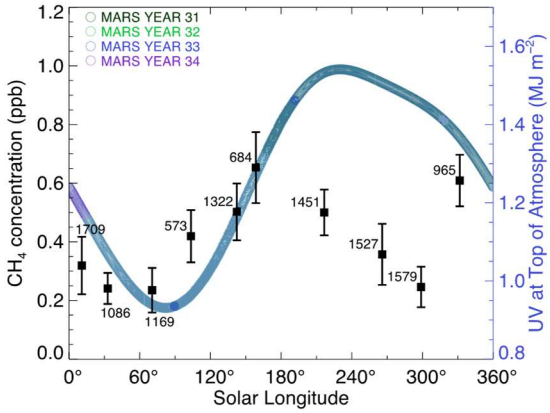

Fig. S7. As Fig. S4, but compared with UV top-of-atmosphere insolation (colored circles).

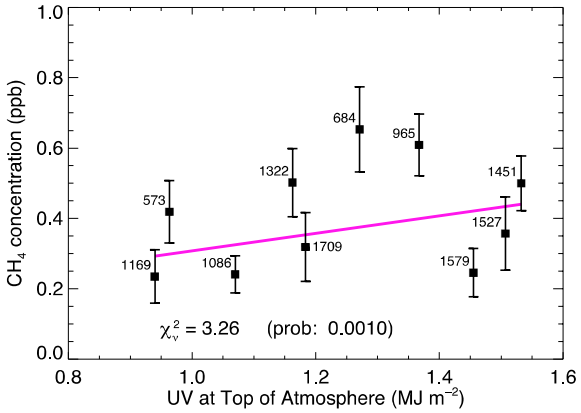

Fig. S8. As Fig. S5, but for correlation with UV top-of-atmosphere insolation. The high χ_ν^2 and probability << 0.1 mean it is not likely there is a simple linear relationship between atmospheric CH_4 concentration and surface UV insolation.

Correlation with UV absorbed within the atmosphere

The motivation for testing the UV insolation per sol absorbed by the atmosphere is that if organics are present in airborne dust, the amount of UV absorbed by the dust could control the production of methane. This environmental variable is close to the difference between the TOA UV and the UV incident at the surface.

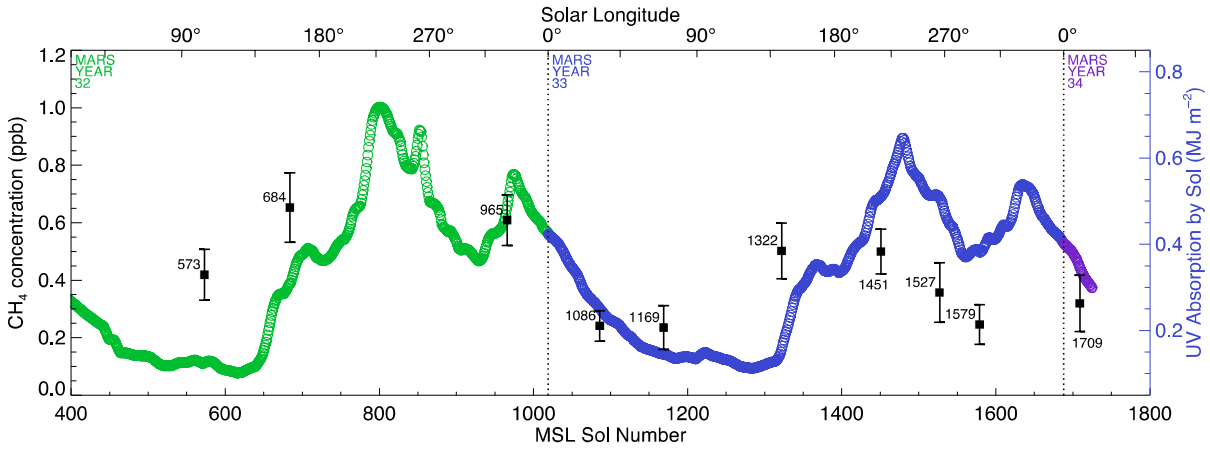

Fig. S9. As Fig. S3, but compared with atmospheric absorbed UV insolation (colored circles).

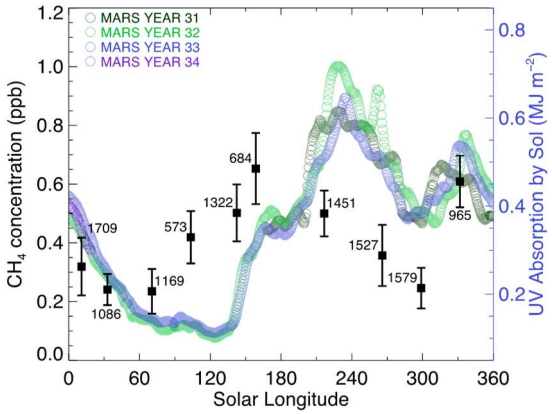

Fig. S10. As Fig. S4, but compared with atmospheric absorbed UV insolation (colored circles).

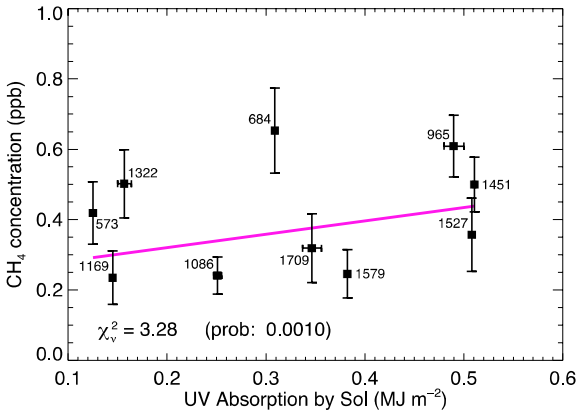

Fig. S11. As Fig. S5, but for correlation with atmospheric absorbed UV insolation. The high χ_ν^2 and probability << 0.1 mean it is not likely there is a simple linear relationship between atmospheric CH_4 concentration and atmospheric absorbed UV insolation.

Correlation with atmospheric dust opacity

Atmospheric dust opacity is measured by Mastcam atmospheric imaging data at 880 nm *(52, 53)*. The data measure attenuation of solar radiation, as well as forward scattering near the sun in the sky, allowing retrieval of particle column densities *(52, 53)*. The motivation for testing this variable is that if organics are present in airborne dust, then higher dust opacities in the atmosphere could mean more surface area of exposed organics.

Solar UV extinction in the atmosphere is dominated by dust, so the absorbed UV insolation shown in Figs. S3–S5 is very closely related to dust optical depth. Thus, features in Figs S3 and S4 are similar to patterns in Figs S12 and S13.

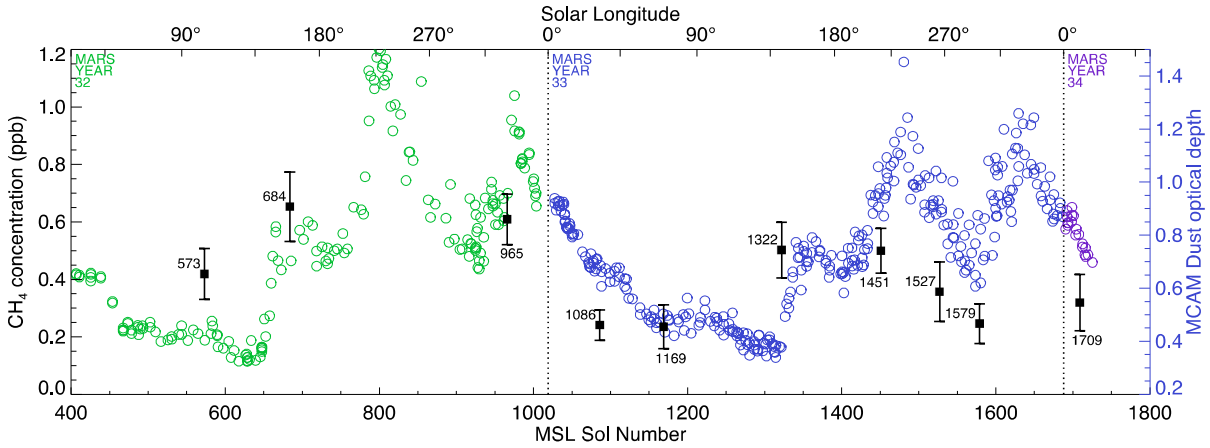

Fig. S12. As Fig. S3, but compared with dust optical depth (colored circles).

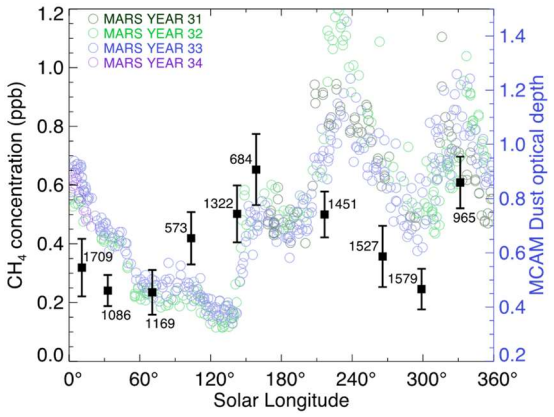

Fig. S13. As Fig. S4, but compared with dust optical depth (colored circles).

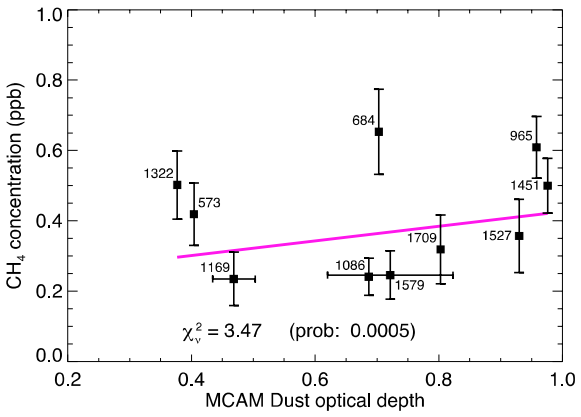

Fig. S14. As Fig. S5, but for correlation with dust optical depth The high $\chi\nu^2$ and probability << 0.1 mean it is not likely there is a simple linear relationship between atmospheric CH_4 concentration and dust optical depth.

Correlation with max atmospheric pressure per sol

Atmospheric pressure varies greatly over each sol, and over the martian year. The REMS pressure sensors measure pressure throughout each sol *(50)*, and the maximum pressure for each sol (occurring late at night) is listed here. We observe a weak, tentative anticorrelation between background CH_4 concentration and maximum pressure. To visually emphasize this anticorrelated (rather than correlated) relationship, we reverse the pressure ordinate scale (right y-axes) so that high CH_4 concentrations are aligned with low maximum pressure per sol. The motivation for testing this variable is that if methane is diffusing from sources partially sheltered from direct atmospheric exposure, there could be a stronger pressure differential when atmospheric pressure is low, leading to a higher release of methane.

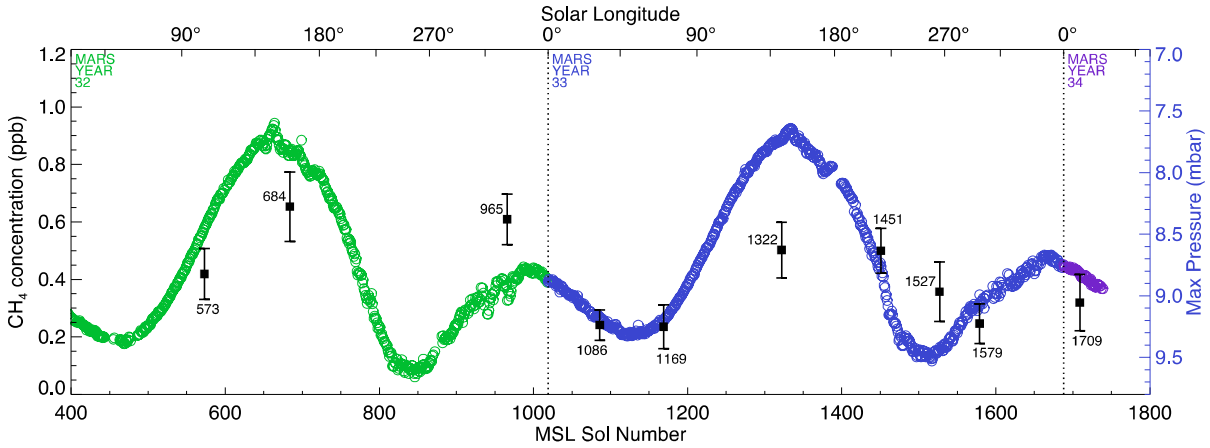

Fig. S15. As Fig. S3, but compared with maximum pressure per sol (colored circles).

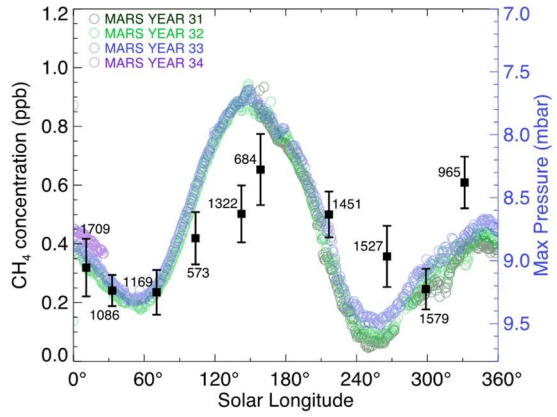

Fig. S16. As Fig. S4, but compared with maximum pressure per sol (colored circles).

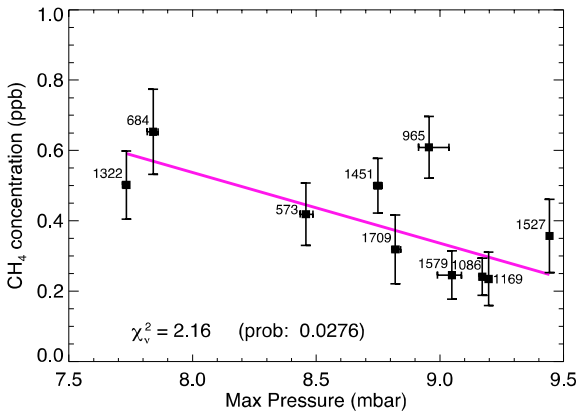

Fig. S17. As Fig. S5, but for correlation with maximum pressure per sol. The high $\chi\nu^2$ and probability < 0.1 mean it is not likely there is a simple linear relationship between atmospheric CH_4 concentration and maximum pressure per sol, although the correlation is better than for most other environmental variables.

Correlation with max ground temperature per sol

Ground temperature is measured by thermal infrared photometers in the REMS package *(50)*. Maximum temperatures per sol occur near midday. The motivation for testing this variable is that if methane is trapped in a volatile condensed reservoir, perhaps below the surface, there could be thermal controls on the communication between the reservoir and the atmosphere. Thermal effects could open/close channels between the reservoir and the atmosphere, either by stressing rock material to create or seal cracks, or by thickening/thinning ice barriers. Clathrate stability is a function of temperature, so CH_4 could be released/trapped in clathrates depending on temperature.

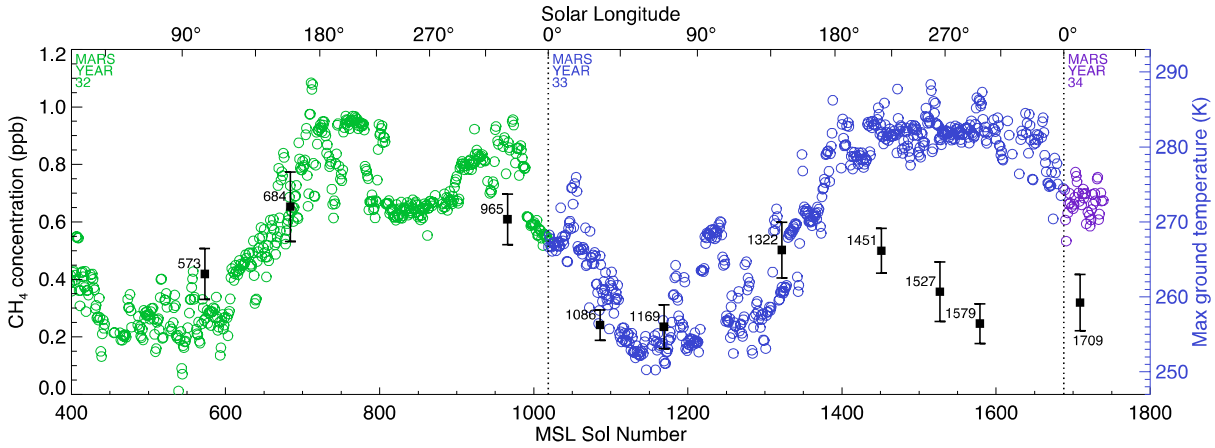

Fig. S18. As Fig. S3, but compared with maximum ground temperature (colored circles). The correlation seems much more convincing at sols < 1400, but the later measurements rule this environmental variable as a major control on CH_4 concentration.

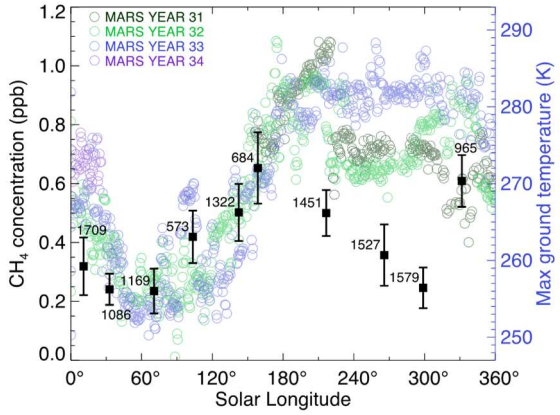

Fig. S19. As Fig. S4, but compared with maximum ground temperature (colored circles). Correlation is better in spring/summer than in fall/early winter.

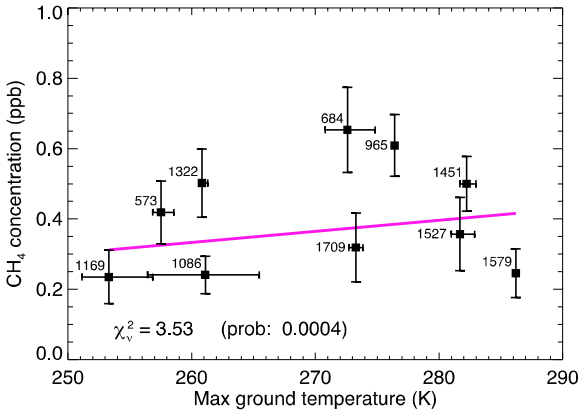

Fig. S20. As Fig. S5, but for correlation with maximum ground temperature. The high $\chi\nu^2$ and probability << 0.1 mean it is not likely there is a simple linear relationship between atmospheric CH_4 concentration and maximum ground temperature.

Correlation with minimum ground temperature per sol

Minimum ground temperatures per sol occur in the middle of the night. The motivation for testing this variable is similar to the motivation for testing maximum ground temperature. If either maximum or minimum had a better correlation, that could be a clue to the nature of the thermal effect governing CH_4 release.

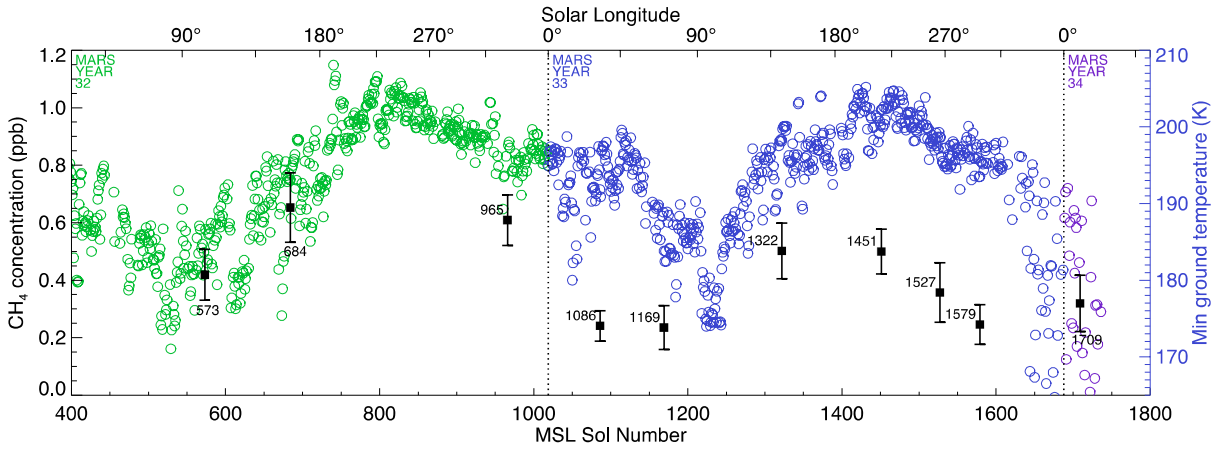

Fig. S21. As Fig. S3, but compared with minimum ground temperature per sol (colored circles).

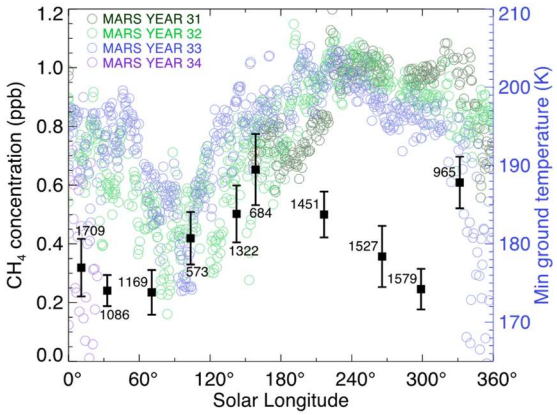

Fig. S22. As Fig. S4, but compared with minimum ground temperature (colored circles).

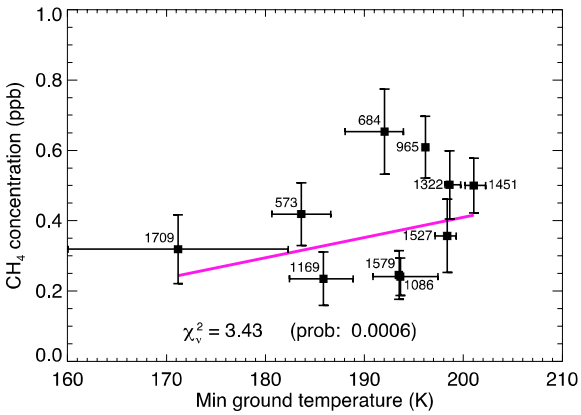

Fig. S23. As Fig. S5, but for correlation with minimum ground temperature. The high $\chi\nu^2$ and probability << 0.1 mean it is not likely there is a simple linear relationship between atmospheric CH_4 concentration and minimum ground temperature.

Correlation with maximum relative humidity (RH) per sol

Relative humidity is directly measured by the REMS meteorology package *(50)*. The motivation for testing this variable is that water and methane volatile cycles may share some similarities in terms of transport or reservoirs. The maximum per sol was chosen as the RH parameter because the REMS sensor is more accurate at higher RH values. To visually emphasize this anticorrelated (rather than correlated) relationship, we reverse the pressure ordinate scale (right y-axes) so that high CH_4 concentrations are aligned with low maximum relative humidities per sol.

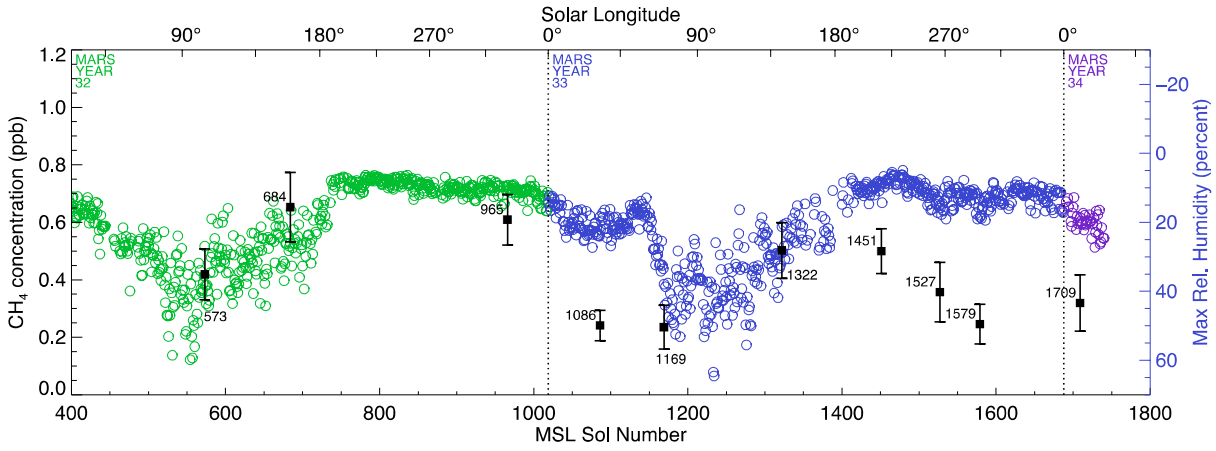

Fig. S24. As Fig. S3, but compared with maximum relative humidity per sol (colored circles).

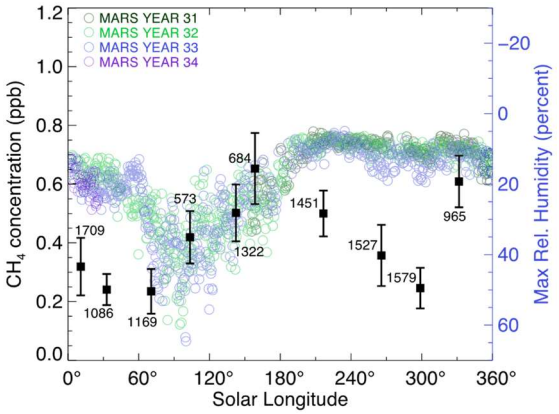

Fig. S25. As Fig. S4, but compared with max RH (colored circles).

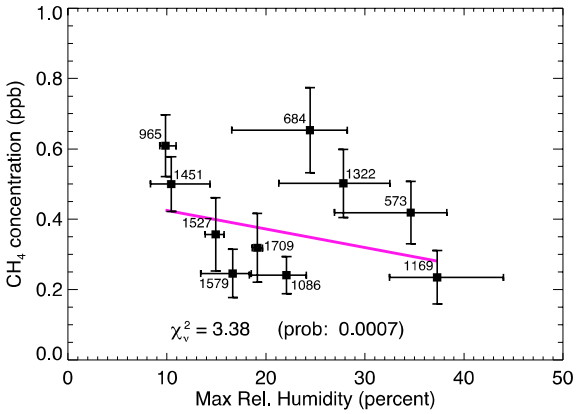

Fig. S26. As Fig. S5, but for correlation with max RH. The high χ_ν^2 and probability << 0.1 mean it is not likely there is a simple linear relationship between atmospheric CH_4 concentration and max RH.

Correlation with H_2O volume mixing ration (VMR)

Using REMS pressure/temperature data, we convert RH to volume mixing ratio. Volume mixing ratio (VMR), or mole fraction, is a temperature-independent measurement of the water content in the atmosphere.

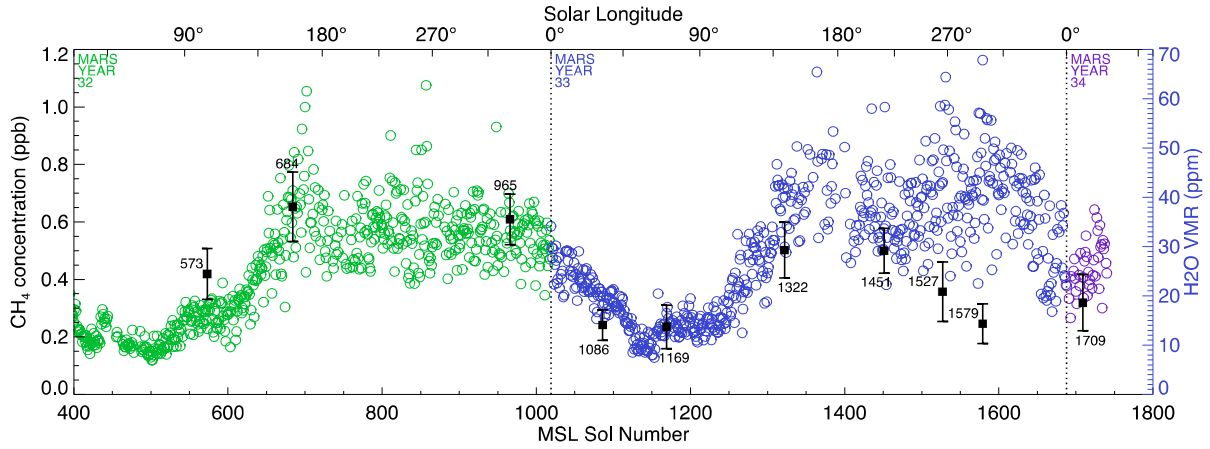

Fig. S27. As Fig. S3, but compared with H_2O VMR (colored circles).

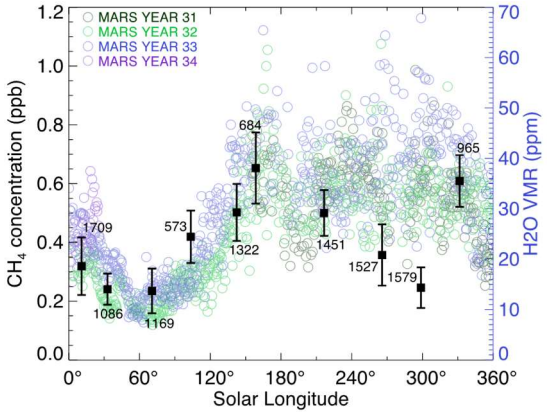

Fig. S28. As Fig. S4, but compared with H_2O VMR (colored circles).

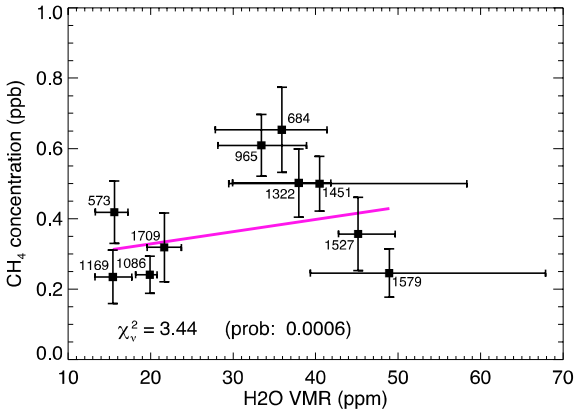

Fig. S29. As Fig. S5, but for correlation with H_2O VMR. The high χ_ν^2 and probability << 0.1 mean it is not likely there is a simple linear relationship between atmospheric CH_4 concentration and H_2O VMR.

Correlation with RAD energetic particle dose rate

The Radiation Assessment Detector (RAD) measures the dose of energetic particle radiation at the MSL rover *(54, 55)*. The motivation for testing this variable is that variation in particle radiation could potentially affect the conversion of organic material to CH_4. RAD values shown in Figs. S30–S32 were measured by RAD within one sol of the TLS methane measurements. In general, unlike the methane measurements, the energetic particle dose rate has increased over time during the mission. To visually emphasize this anticorrelated (rather than correlated) relationship, we reverse the pressure ordinate scale (right y-axes) so that high CH_4 concentrations are aligned with low radiation doses.

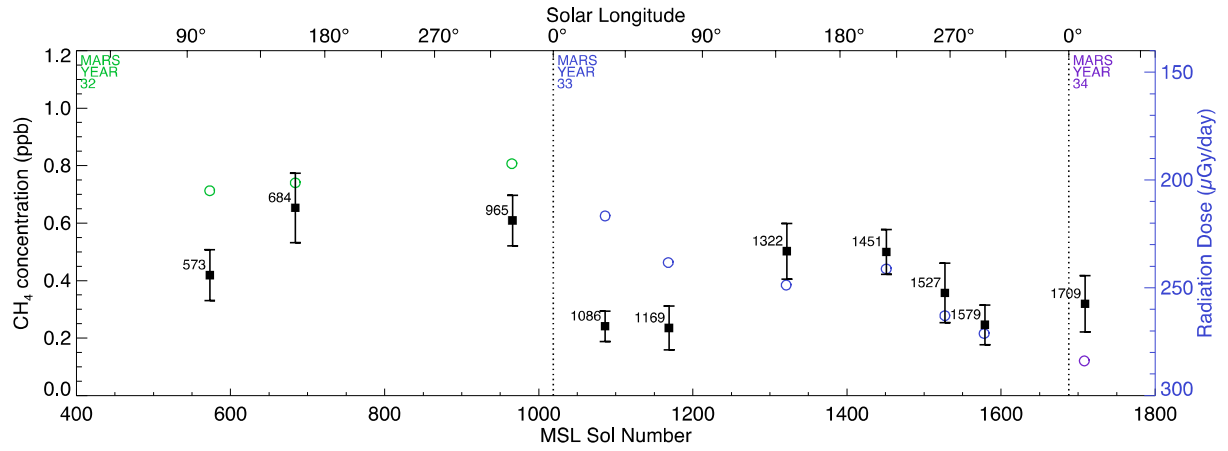

Fig. S30. As Fig. S3, but compared with energetic particle radiation dose (colored circles). RAD measurements in Mars years 33 and 34 are higher than previous measurements, suggesting that the variation is not seasonal in nature *(56, 57)*.

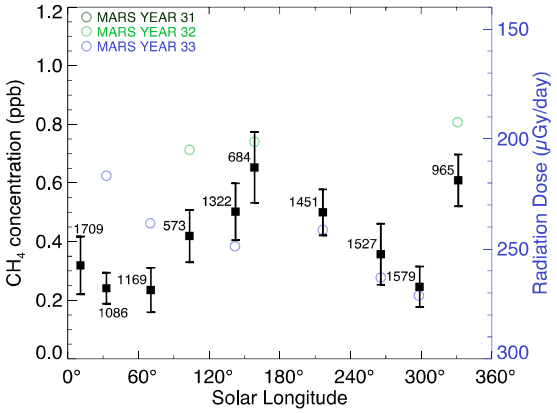

Fig. S31. As Fig. S4, but compared with energetic particle radiation dose (colored circles).

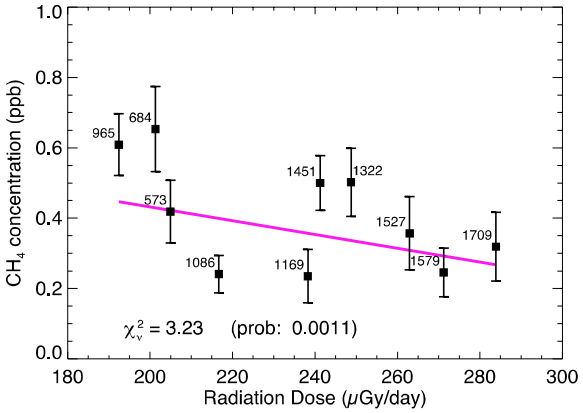

Fig. S32. As Fig. S5, but for correlation with energetic particle radiation dose. The high $\chi\nu^2$ and probability << 0.1 mean it is not likely there is a simple linear relationship between atmospheric CH_4 concentration and energetic particle radiation dose.

Correlation with SAM/QMS argon measurements (with pressure correction)

SAM/QMS has measured argon's seasonal variation, but measurements were done in separate experimental runs from the SAM/TLS CH_4 measurements *(58, 59)*. There are irregular gaps in time between measurements of Ar and CH_4. To test correlations, we first performed a 2-parameter fit to argon's seasonal variation (Fig. S34). The fitting function is of the form:

$$Y = A + B \times \sin(2L_S) \quad \text{(S1)}$$

and does not capture differences in the depth of the minima near L_S 45° and 220°, nor the maxima near L_S 130° and 315°. Still, the fit is sufficient to allow a test of the correlation between Ar and CH_4 (Fig. S35), despite the time separation between measurements of these gases.

Argon volume mixing ratios (VMRs) plotted here have been corrected for pressure variation to correspond to global mean annual mixing ratios (i.e., multiplied by a Fp factor as in Table S2). The amplitude of the seasonal argon variation is much lower than the amplitude of the CH_4 variation. The two gases are anti-correlated (so the y-axis of Figs. S33 and S34 are inverted), but the statistical significance of their linear correlation is poor.

Argon VMRs in Figures S33–S35 and S36–S38 (from *(58)*) are all normalized to their maximum value.

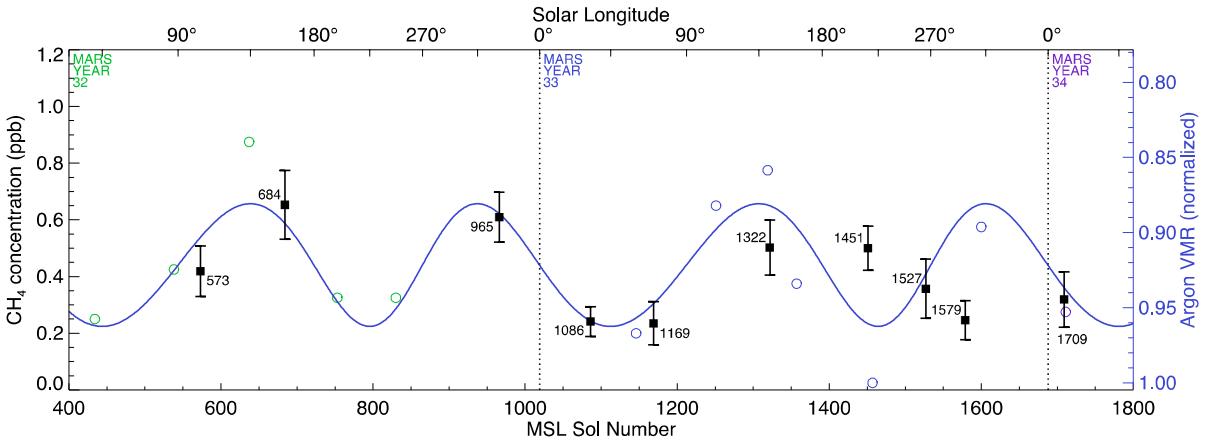

Fig. S33. As Fig. S5, but compared with argon VMR (colored circles) and a crude continuous fit (solid color curve). SAM/QMS argon measurements are from *(58)*.

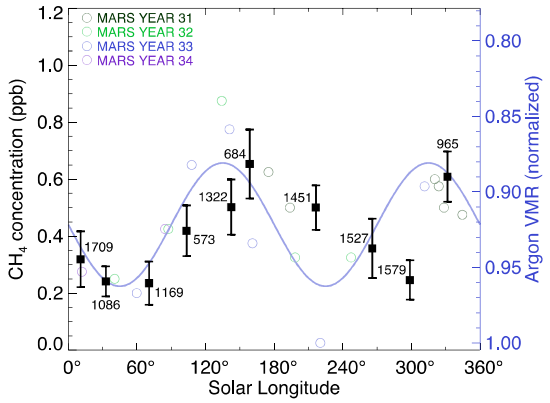

Fig. S34. As Fig. S6, but compared with argon VMR (colored circles) and a crude continuous fit (solid color curve).

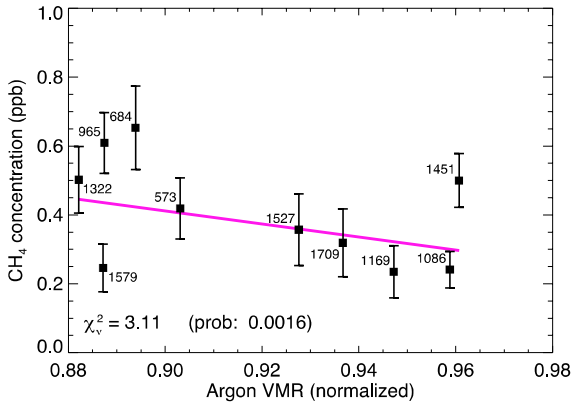

Fig. S35. As Fig. S7, but for correlation with the continuous fit to argon seasonal variation shown in Figs. S33 and S34. Errors from the argon seasonal fitting procedure are not taken into account.

Correlation with SAM/QMS argon measurements (without pressure correction)

We attempted another comparison between CH_4 and argon, without the pressure correction that converts instantaneous volume mixing ratios to global annual mean mixing ratios (i.e., multiplication by Fp in Table S2). The observed (uncorrected) values in Figure S37 show similar seasonal trends between argon and CH_4. The pressure correction removes most, but not all, of this variation for argon (Fig. S34), while CH_4 is only slightly modified, due to its higher-amplitude signal. The uncorrected argon and CH_4 variations are correlated, while the pressure-corrected argon and CH_4 variations are anti-correlated. To compare the two gases, we performed a 3-parameter fit to argon's seasonal variation (Fig. S37), of the form

$$Y = A + B \times \cos(L_S) + C \times \cos^2(L_S) \qquad (S2)$$

This function does not capture differences in the depth of the minima near L_S 70° and 290°, but still, the fit is sufficient to allow correlations between uncorrected Ar and CH_4 to be tested (Fig. S38), despite the time separation between measurements of these gases.

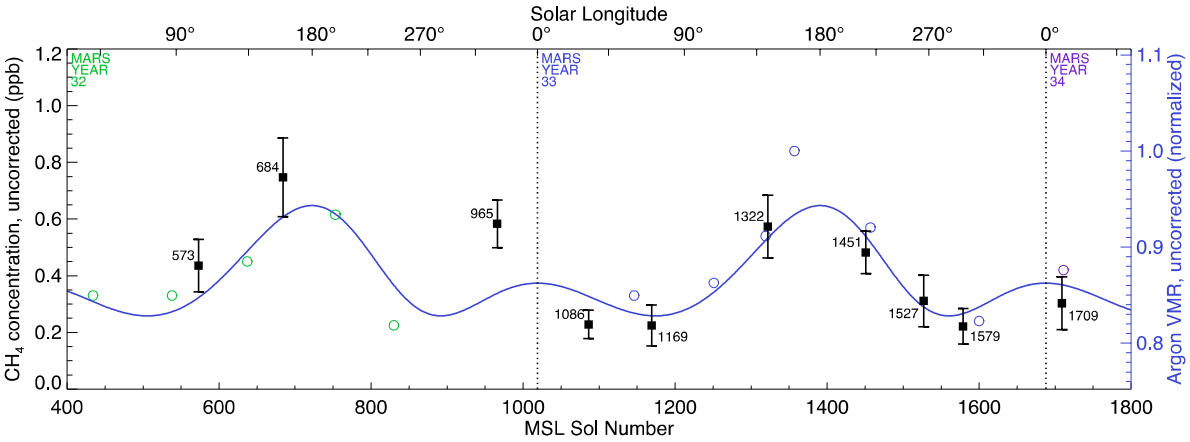

Fig. S36. As Fig. S33, but for Ar and CH_4 measurements without pressure correction.

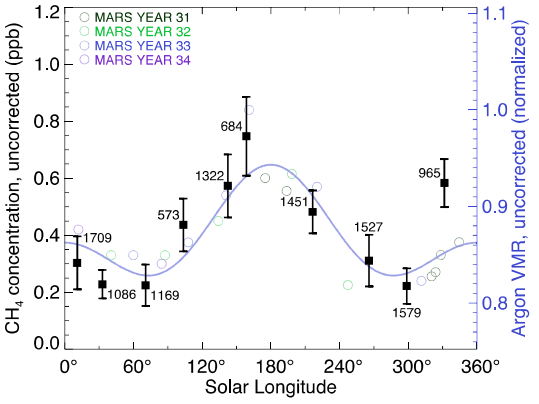

Fig. S37. As Fig. S34, but compared with argon VMR (colored circles) and a crude continuous fit (solid color curve).

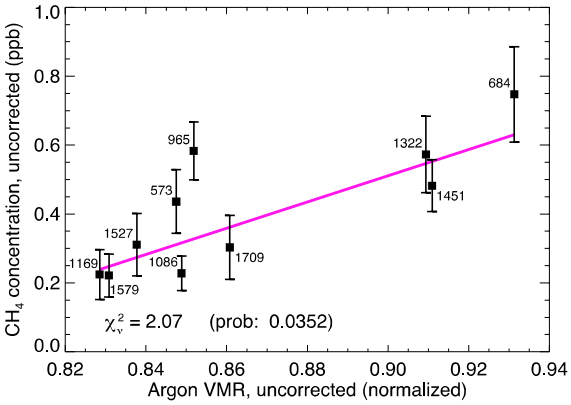

Fig. S38. As Fig. S7, but for correlation with the continuous fit to argon seasonal variation shown in Figs. S33 and S34.

If CH_4 were simply an inert long-lived gas like Ar then, within error bars, their variation over the Martian year would be correlated. The correlation between the uncorrected CH_4 and the uncorrected Ar mixing ratios (Figs S37 and S38) shows the importance of the pressure correction as both gases are non-condensable gases with respect to CO_2 over the year. However, after correction for this effect there is an anti-correlation, if any, between CH_4 and Ar (Figs S34 and S35). This suggests processes affecting CH_4 variation that are not seen in the Ar variation.

Supplementary Text

Additional discussion of possible sources: Adsorption and Release of Methane from Surface material

Another possibility is that a surface that is capable of retaining methane temporarily may provide reasonable fits to the data. Such a surface would respond according to an Arrhenius process in ground temperature. Here we consider whether adding such a surface could provide reasonable fits to the data. If that process has an energy barrier of ~20-35 kJ/mol, then large seasonal variations are expected, as shown in Fig. S39. That process could be adsorption on a surface with high specific surface area, e.g. dust or soil. While the mineral dust cannot serve as a significant sink, volumetrically, for the methane *(10, 11)*, it can moderate its release.

The value of 20 kJ/mol is derived from the upper bound of the studies of Gough and others *(10, 11)*. Energy barriers of less than 20 kJ/mol cannot provide the required range of methane values from a simple surface to explain the variation seen in the TLS-SAM results. The upper limit of 35 kJ/mol is chosen as energies above this value produce too much variation in the methane concentration for a simple surface, though values of up to ~100 kJ/mol for water regolith systems have been described in the literature *(60)*. The energy barrier required to match seasonal methane variations measured by TLS-SAM is consistent with the physical adsorption of methane into clays *(46)*, zeolites *(47)*, and JSC-Mars-1 analog soil *(11)*. Although difficult to achieve the large seasonal methane variations observed by TLS-SAM, it is possible to achieve absolute amounts close to the observed mean value without a very large subsurface methane reservoir.

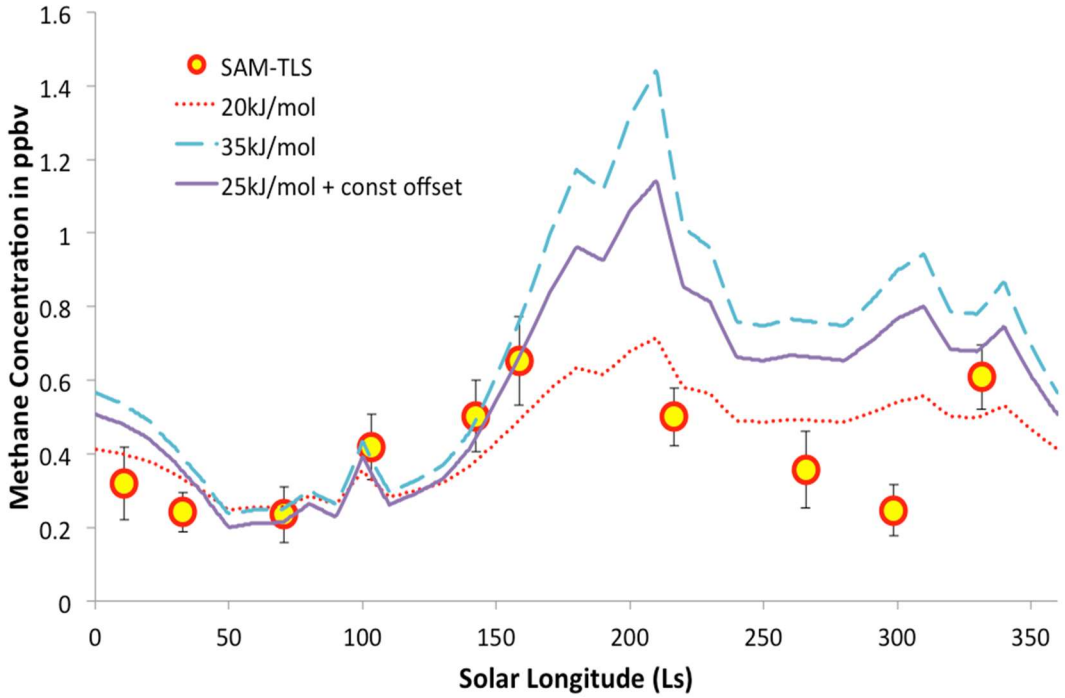

Fig. S39. Arrhenius-like processes with energy barriers between 20-35 kJ/mol may provide reasonable fits to the data. The symbols with error bars are the SAM-TLS data of Fig. 1B, and the lines are the model calculations for various activation energies as described below.

The curves shown in Fig. S39 above are plotted corresponding to:

$$p = A\sqrt{T}\exp\left({}^{-E_a}/_{RT}\right) - p_0 \qquad \text{(S3)}$$

Where p is pressure, expressed as a concentration (ppbv), p0 is an assumed constant baseline or offset pressure, again expressed as a concentration, T is temperature, Ea is activation energy/energy barrier and R is the universal gas constant.

This formulation is chosen by analogy to the rate constants for adsorptive processes, e.g. *(11)*, which yield equilibrium gas-phase pressure when combined with a constant surface coverage of methane which has a very low surface coverage, e.g. $\theta \cong p\, k_{eq}$. Three sample curves are provided. For the curve of E_a = 20 kJ/mol, $A = 2\times10^2$ ppbv and $p_0 = 0$. For the curve of E_a = 35 kJ/mol, $A = 2.3\times10^5$ ppbv and $p_0 = 0$. For the curve of E_a = 25 kJ/mol, $A = 3\times10^3$ ppbv and $p_0 =$ 0.15 ppbv. The curve with E_a = 20 kJ/mol provides the necessary amplitude seen in the data while that with E_a = 35 kJ/mol is better able to replicate the ramp-up and ramp down needed to match the points near 158.8º and 331º. If a non-zero constant offset is permitted, better fits are obtained at lower adsorption energies, as demonstrated by the purple curve. The temperatures chosen are daily maximum values given by REMS data and are 2-year smoothed averages following the landing, while Curiosity roved upon the plains of Gale crater.

Assessing the Curiosity Rover as a Potential Source of Measured Methane:
By their very architecture, in situ measurements are subject to potential contamination issues that must be rigorously ruled out or their contribution accurately measured. This is particularly true when low abundance signals are being retrieved. Concern has been expressed *(35)* over the possibility that the Curiosity rover itself has unknown or hidden sources of methane that might vent to produce methane around the rover which is then detected by TLS-SAM. The only known source of contaminant methane on the rover is the terrestrial methane residing in the TLS-SAM foreoptics chamber *(35)*). Zahnle *(35)* was concerned about the terrestrial methane residing in the TLS-SAM foreoptics chamber, noting "…the rover contains within a chamber some methane at a concentration 1,000 times higher than the puff supposedly found in Mars' atmosphere. Curiosity's methane comes from Earth." Zahnle was also concerned about other potential rover sources.

Regarding the measurement geometry, SAM is a microwave oven-sized instrument suite (see Fig. S40 below) residing in the belly of the rover. SAM comprises a myriad of tubing and chambers and cabling connected to two turbomolecular pumps for feeding or pumping the TLS (and QMS, GC) instrument, and driving a sample handling system for oven pyrolysis of rock samples. While contained within a metallic structure (box), the box is not hermetically sealed so that the inside of the box follows the Mars atmospheric pressure through vents (leaks) between the box interior, the rover belly structure and the Mars atmosphere. The outside of internal subsystems like TLS is therefore in contact indirectly with the Mars atmosphere. All plumbing is internally sealed with ultrahigh-vacuum fittings/seals, so that the only Mars atmosphere entry points are the valve-controlled inlet ports on the outside body of the Curiosity rover that control atmospheric ingest or venting. The inlets and the internal SAM suite are all raised to relatively

high temperatures throughout measurement and sampling. The inlets are regulated at 55°C, and the TLS spectrometer head is held at 45°C during all measurements.

For contaminant methane (whether from the Mars atmosphere, evolved from the SAM Evolved Gas Experiments (EGA), from the TLS foreoptics, or from an unknown rover source) to be seen (recorded) by TLS, it must arrive inside the Herriott cell during the short time (~30 mins) the full cell data are collected in between empty cell pumpouts. Because all the TLS and SAM plumbing is enclosed with high-vacuum seals right up to the inlets, getting contaminant methane into the Herriott cell from an external source is very challenging (unlikely) to begin with.

Although the TLS foreoptics chamber has ~1,000 times the concentration (ppmv mixing ratio) of that measured in the Martian atmosphere (as pointed out by Zahnle), the TLS foreoptics chamber contains ~2 nanomoles, or ~10^{15} molecules of methane (see below). We will refer to this value in a relative comparison of potential methane sources/reservoirs.

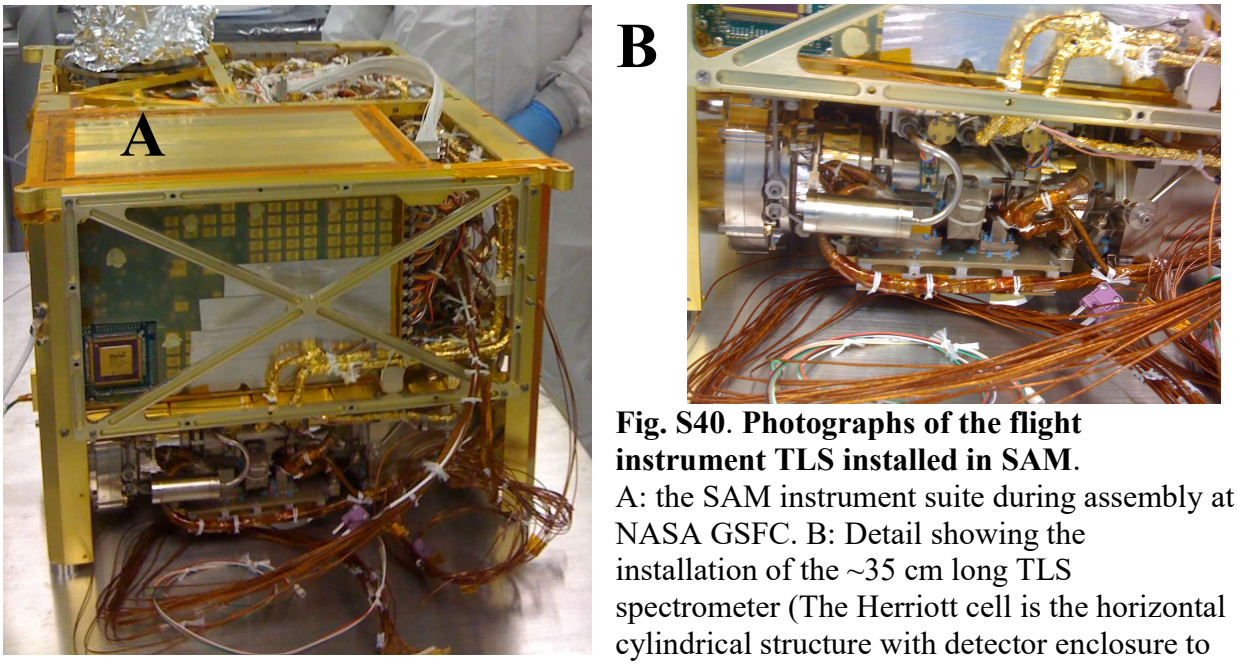

Fig. S40. Photographs of the flight instrument TLS installed in SAM. A: the SAM instrument suite during assembly at NASA GSFC. B: Detail showing the installation of the ~35 cm long TLS spectrometer (The Herriott cell is the horizontal cylindrical structure with detector enclosure to left, and the foreoptics chamber on the right of the photograph).

1. **Could the SAM suite or other rover instrumentation be providing a source of methane shielded from the wind that gets ingested into the inlets?**

Consider the Curiosity rover environment and geometry during the two-month period between Sols 466 and 526 when we detected elevated methane values (~7 ppbv).

To understand the level of contamination needed to dominate the measured values, we consider two hypothetical spheres of atmosphere around or within the rover, one of 1-m diameter, a second of 10-m diameter. A 1-meter diameter sphere around the rover, at a pressure of 7 mbar (mainly CO_2) at typical Mars temperatures and containing 7 ppbv CH_4 will contain ~1 micromole of CH_4, or ~10^{15} molecules of methane. A 10-meter diameter sphere will contain one thousand times this amount, namely ~10^{18} molecules of methane.

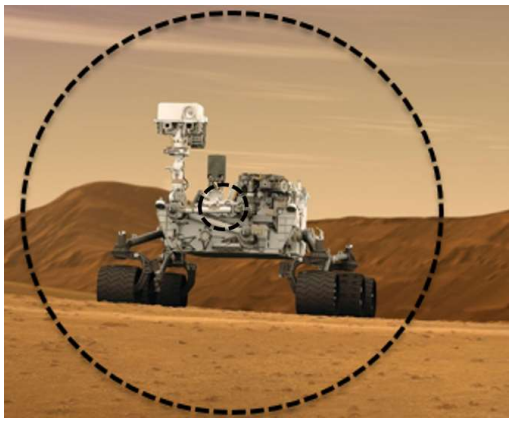

Fig. S41. Two hypothetical spherical "clouds" of air containing 7 ppbv methane in comparison to the Curiosity rover. A sphere of 1-m diameter would contain ~10^{15} molecules of methane, and a 10-m diameter sphere would contain ~10^{18} molecules of methane.

The background image is an artist's impression *(61)*.

In the absence of winds, to maintain a 10-m diameter cloud of contaminant methane at 7 ppbv around the rover during a single TLS measurement would require 10^{18} molecules of methane, or ~1,000 times the total amount of methane in the TLS foreoptics chamber. A smaller contaminant cloud, of only 1-m diameter around the SAM instrument and inlet would require ~10^{15} molecules of methane, i.e. all of the foreoptics methane available. This scenario must then be repeated for the several measurements of ~7 ppbv seen, and then we must factor in replenishment by the near-surface winds of typically 3-5 m/sec *(36)*.

Thus, a source of contaminant methane that somehow gets into the rover environment to be entrained into the SAM inlet during the ingest period would need to be at least ~10 times the total amount of methane in the TLS foreoptics chamber. We rule this possibility out because no such large source of methane has been identified, and also the foreoptics chamber shows no evidence of significant loss over the 5 year mission.

2. **Could the Evolved Gas Experiments (EGA) that are known to produce methane be contaminating the atmospheric measurements?**

During SAM evolved gas analysis (EGA) experiments, Martian rock samples are crushed and heated up (pyrolyzed) in an oven to produce gaseous products for analysis by QMS, GC, and TLS. This includes evolved methane that accompanies the He flow of gas into the TLS sample cell. In most cases, ~1-20 parts-per-million of methane are detected in the TLS Herriott cell.

We considered whether TLS was detecting high CH_4 values in the Martian atmosphere immediately following an EGA-vent occurrence, in which the high CH_4 from EGA (typically ~10 ppmv in He) was vented into the pipe between the TLS cell and the low conductance inlet filter. The idea was that somehow this volume was not well-mixed, so that in days after the EGA-vent, when a new sample was ingested through that stagnant inlet for a direct ingest methane measurement, we somehow entrained these earlier higher values to produce our ~7 ppbv results. However, as Fig. S42 below shows, there is no evidence of this.

For example, our 4 sequential high methane measurements of sols 466-526 are seen after SAM EGA experiments. But with the putative mechanism of residual methane in the entrainment plumbing, we would expect the four measurements to show decreasing values each time, not the increases observed. Also, many other SAM EGA measurements are not followed by high methane values, notably the low CH_4 values immediately following vents near 1130 and 1445 for example in which we had seen very high EGA CH_4 amounts sols before our atmospheric methane measurements. A second example is the high of sol ~1500 that followed a low of Sol 1450 with no EGA in between.

Thus, we rule out the possibility that the Evolved Gas Experiments (EGA) that are known to produce methane are contaminating the atmospheric measurements.

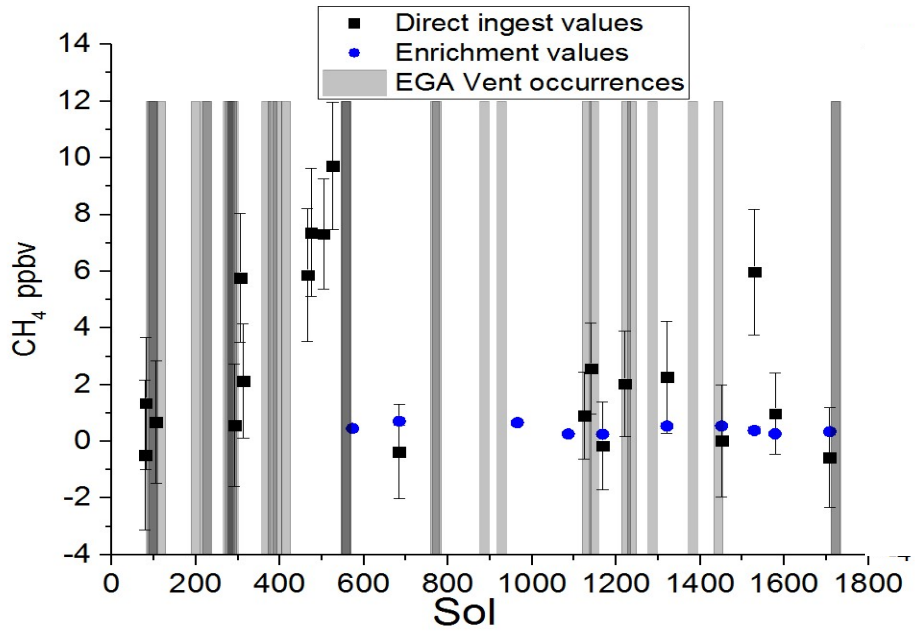

Fig. S42. Comparison of all TLS-SAM methane measurements to May 27th 2017 (Table S2) with evolved gas analysis (EGA) runs. Times at which EGA runs were done are indicated with a thin grey vertical line. Multiple EGA runs done in short succession produce thicker, darker vertical lines.

3. Could the foreoptics terrestrial methane be leaking directly into the Herriott cell and therefore providing a source of measured methane?

Under this scenario, foreoptics gas containing methane (present at parts-per-million levels) would leak directly into the Herriott cell during the measurements.

Foreoptics Methane Behavior:

To assess foreoptics leakage and its potential effect on measurements, we first describe the observed behavior of the foreoptics over time, noting that the foreoptics pressure is measured every 3 seconds that SAM is running (see Fig. S43 plot below for long-term trend, that uses run-averages). Apart from two deliberate attempts to reduce that pressure (pump out the chamber)

there is no evidence of a broken seal or large leakage of gas out of the foreoptics chamber over the 5 years of measurements.

The empty cell measurements used in our difference method provide each time a direct measurement of the foreoptics methane amount that we plot below in Fig. S43. That amount has varied somewhat during pumping attempts, but as shown below, remains around ~2 nanomoles, or ~10^{15} molecules of methane in the foreoptics chamber.

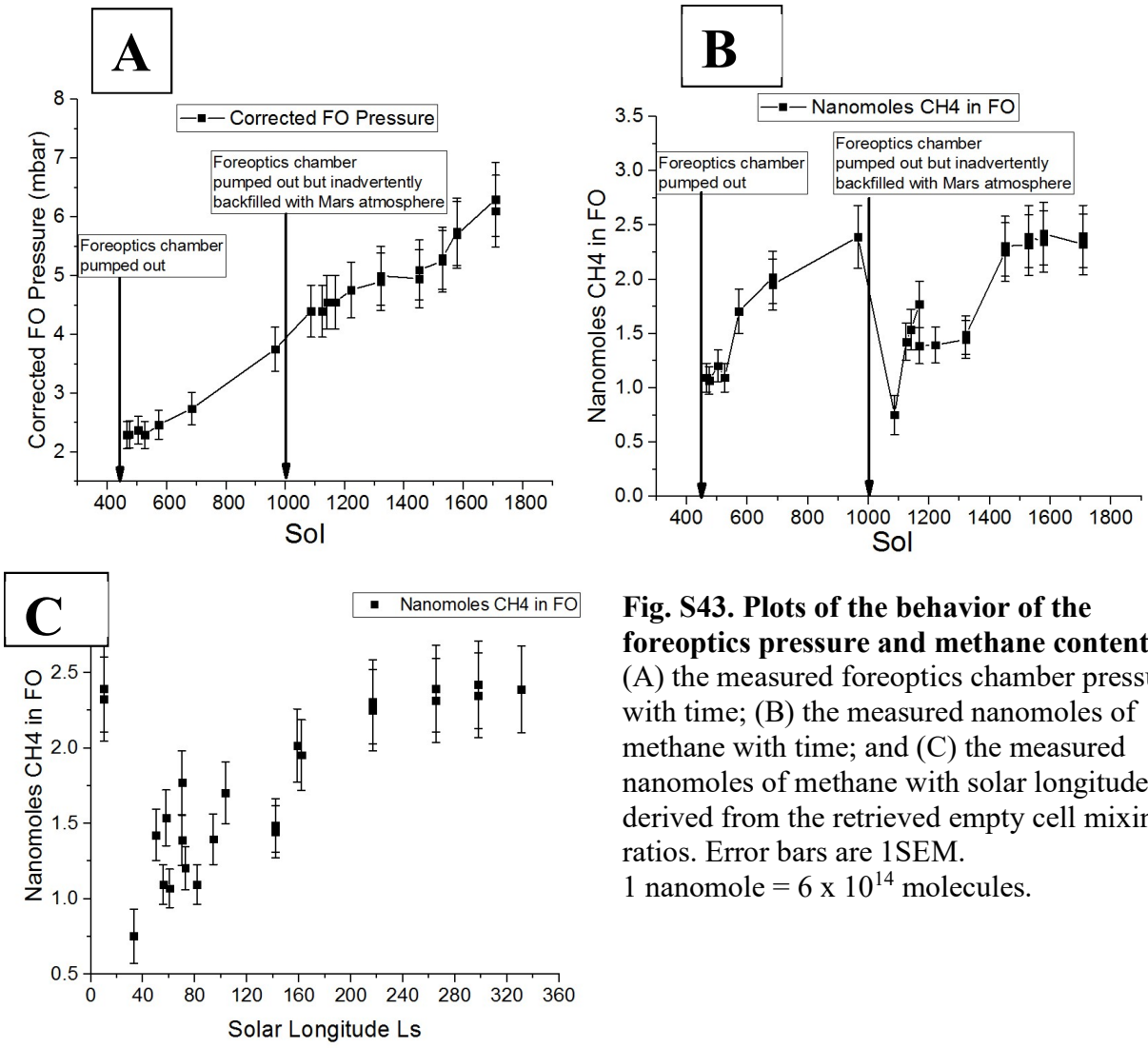

Fig. S43. Plots of the behavior of the foreoptics pressure and methane content. (A) the measured foreoptics chamber pressure with time; (B) the measured nanomoles of methane with time; and (C) the measured nanomoles of methane with solar longitude derived from the retrieved empty cell mixing ratios. Error bars are 1SEM.
1 nanomole = 6 x 10^{14} molecules.

Fig. S43A shows that following a pump-out near sol 400, the foreoptics pressure slowly rises toward Mars ambient pressure as the Mars atmosphere (mainly CO_2) permeats the foreoptics external seal. Then, at sol 1000 we again pumped out the foreoptics but inadvertently backfilled it to about 4 mbar of Mars atmosphere. This is why the pressure plot on the top left shows little change, but the methane content in the top right plot has been reduced significantly. Following both pump-outs, the methane content of the foreoptics chamber (Fig. S43B) generally grows to an equilibrium value near 2.2 nanomoles. The slow growth in the foreoptics amount may be due

to equilibrium settling with a small amount of methane being released from the epoxy and cabling inside the chamber.

Foreoptics Chamber Leak Rates:

The leak rates across the various seals in the TLS spectrometer were modelled and measured in pre-launch studies of the assembled flight instrument. The highest leak rate is from the outside (~7 mbar) gas into the foreoptics chamber through electrical pins and connectors, laser plate seals, valves etc. The second highest leak rate is from the foreoptics chamber directly into the Herriott cell through the wedge window and mirror o-ring seals: this rate was found to be ~100 times less than that from the outside into the foreoptics chamber. From Fig S43A, the foreoptics chamber pressure increases from ~2 to ~4 mbar over 700 sols. This is equivalent to a leak rate from the outside into the foreoptics chamber of $\sim 10^{-8}$ standard cubic centimeters (scc)/sec which for the differential pressure of 4 mbar agrees with pre-launch estimates. This external seal is behaving as expected. If the Mars atmosphere permanently contained 7 ppbv methane that accompanied the mainly CO_2 leaking into the foreoptics chamber, the long-term tripling of the foreoptics pressure shown in Fig. S43A would only cause an increase of <0.1 nanomoles of methane in the foreoptics. Fig. S43B shows that the shape of the seasonal cycle reported is in no way related to the foreoptics methane behavior.

Regarding potential leakage from the foreoptics chamber directly into the Herriott cell, leak rates through o-ring seals are driven by a permeation process *(62)* that occurs in 3 steps: (i) the gas dissolves (adsorbs) onto the near o-ring surface; (ii) the gas diffuses through the solid o-ring according to Fick's law of diffusion; and (iii) the gas then desorbs from the far o-ring surface. The permeation rate depends on the o-ring permeation coefficient and area, and is inversely proportional to the o-ring thickness, and proportional to the pressure gradient. This latter pressure gradient refers to a pure gas (often nitrogen or helium) and actually represents the concentration gradient. For the TLS instrument, the leak rate from foreoptics chamber to Herriott cell will be driven by the concentration gradient occurring from the high methane concentration in the foreoptics chamber (ppmv) against the low concentration (ppbv) in the Herriott cell. Should such a leak be present, we would expect all the empty cell plot and the full cell plot data points (one every 30 seconds) to show gradual increase in time during the 26-point data collections. This is not observed as shown below.

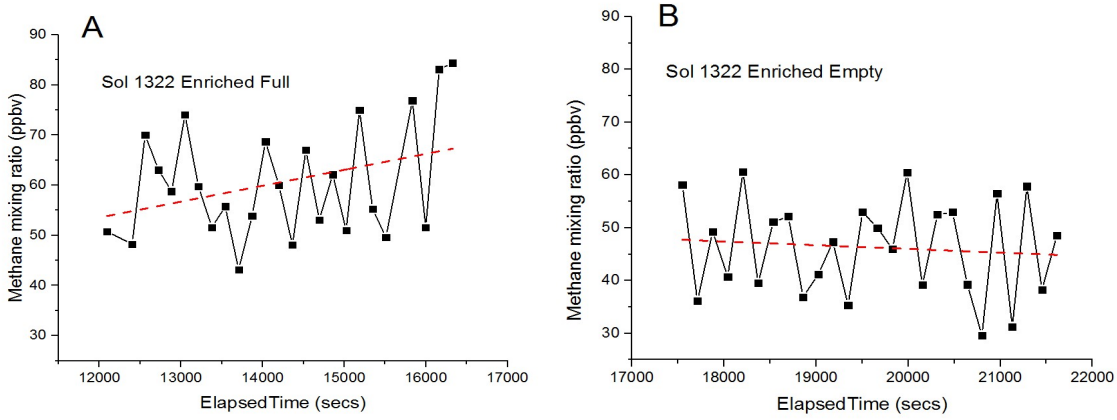

Fig. S44. Example trend plot for sol 1322 data of the full cell (A) and empty cell (B) measurements taken every 30 seconds. Wefg in each case is the methane mixing ratio in ppbv

and the red line a linear fit to the data. With a foreoptics leak, both empty and full data sets should show an increase with elapsed time; here they do not, and actually show opposite trends. Using the mean values, we would calculate a difference of 60.25-46 =14.25 ppbv that when divided by the EF of 25 would produce a Mars value of 0.57 ppbv as reported in Tables 1 and S2.

Most trend plots are flat, while some show minor trends up or down (see Fig. S44 example) that are attributed to changes in the rate of change of the laser plate temperature that cause slight changes in the retrieved mixing ratio due to minor spectral blurring during the on-board spectral averaging over the 30-second period for each point. Analysis of empty and full cell trends shows no significant change (up or down) of the retrieved mixing ratios with time, as shown in the example of Sol 1322 of Fig. S44.

Our "daytime" measurement offers an independent confirmation of the lack of foreoptics chamber leak into the Herriott cell. For the sol 305 measurement given in Table S2 that reported a mixing ratio of ~5.8 ppbv, the Herriott cell was filled during the daytime. Due to constraints in the daytime energy budget, this sample was left in the Herriott cell for ~12 hours until TLS could be turned back on at night to make the measurement. If we were to assume that all this methane came from a foreoptics chamber leak into the Herriott cell over the long static period of 12 hours, then we would expect our normal (enrichment) run periods of 30 minutes to accumulate ~5.8/24 = 0.24 ppbv, which when divided by the enrichment factor of 25 would contribute only ~0.01 ppbv to our typical (~0.4 ppbv) enrichment result. This result sets a useful upper limit to the contribution that supports the lack of trend seen in the individual runs.

As described above, we rule out the possibility of a direct leak of foreoptics methane into the Herriott cell. The difference method (full cell minus empty cell over a relatively short duration) mitigates against the possibility of a direct transfer.

From the data plotted above in Fig. S43, we conclude that there is no evidence of long term loss of significant amounts methane from the TLS foreoptics chamber and therefore do not believe it to be a source of contamination to our atmospheric measurements.

References and Notes

1. S. K. Atreya, P. R. Mahaffy, A. S. Wong, Methane and related trace species on Mars: Origin, loss, implications for life, and habitability. *Planet. Space Sci.* **55**, 358–369 (2007). doi:10.1016/j.pss.2006.02.005

2. Core Writing Team, Intergovernmental Panel for Climate Change (IPCC), *Fifth Assessment Report 2014*, R. K. Pachauri, L. A. Meyer, Eds. (IPCC, 2014); www.ipcc.ch.

3. V. A. Krasnopolsky, J. P. Maillard, T. C. Owen, Detection of methane in the martian atmosphere: Evidence for life? *Icarus* **172**, 537–547 (2004). doi:10.1016/j.icarus.2004.07.004

4. M. J. Mumma, G. L. Villanueva, R. E. Novak, T. Hewagama, B. P. Bonev, M. A. Disanti, A. M. Mandell, M. D. Smith, Strong release of methane on Mars in northern summer 2003. *Science* **323**, 1041–1045 (2009). doi:10.1126/science.1165243 Medline

5. C. Oze, M. Sharma, Have olivine, will gas: Serpentinization and the abiogenetic production of methane on Mars. *Geophys. Res. Lett.* **32**, L10203 (2005). doi:10.1029/2005GL022691

6. F. Keppler, I. Vigano, A. McLeod, U. Ott, M. Früchtl, T. Röckmann, Ultraviolet-radiation-induced methane emissions from meteorites and the martian atmosphere. *Nature* **486**, 93–96 (2012). doi:10.1038/nature11203 Medline

7. A. Schuerger, J. E. Moores, C. A. Clausen, N. G. Barlow, D. T. Britt, Methane from UV-irradiated carbonaceous chondrites under simulated martian conditions. *J. Geophys. Res.* **117**, E08007 (2012). doi:10.1029/2011JE004023

8. V. A. Krasnopolsky, Some problems related to the origin of methane on Mars. *Icarus* **180**, 359–367 (2006). doi:10.1016/j.icarus.2005.10.015

9. E. Chassefière, Metastable methane clathrate particles as a source of methane to the martian atmosphere. *Icarus* **204**, 137–144 (2009). doi:10.1016/j.icarus.2009.06.016

10. P.-Y. Meslin, R. Gough, L. Lefevre, F. Forget, Little variability of methane on Mars induced by adsorption in the regolith. *Planet. Space Sci.* **59**, 247–258 (2010). doi:10.1016/j.pss.2010.09.022

11. R. V. Gough, M. A. Tolbert, C. P. McKay, O. B. Toon, Methane adsorption on a martian soil analog: An abiogenic explanation for methane variability in the martian atmosphere. *Icarus* **207**, 165–174 (2010). doi:10.1016/j.icarus.2009.11.030

12. S. McMahon, J. Parnell, N. J. F. Blamey, Sampling methane in basalt on Earth and Mars. *Int. J. Astrobiol.* **12**, 113–122 (2013). doi:10.1017/S1473550412000481

13. G. Etiope, D. Z. Oehler, C. C. Allen, Methane emissions from Earth's degassing: implications for Mars. *Planet. Space Sci.* **59**, 182–195 (2011). doi:10.1016/j.pss.2010.06.003

14. E. S. Kite, P. Gao, C. Goldblatt, M. A. Mischna, D. P. Mayer, Y. L. Yung, Methane bursts as a trigger for intermittent lake-forming climates on post-Noachian Mars. *Nat. Geosci.* **10**, 737–740 (2017). doi:10.1038/ngeo3033

15. G. L. Villanueva, M. J. Mumma, R. E. Novak, Y. L. Radeva, H. U. Käufl, A. Smette, A. Tokunaga, A. Khayat, T. Encrenaz, P. Hartogh, A sensitive search for Organics (CH_4,

CH_3OH, H_2CO, C_2H_6, C_2H_2, C_2H_4), hydroperoxyl (HO_2), nitrogen compounds (N_2O, NH_3, HCN) and chlorine species (HCl, CH_3Cl) on Mars using ground-based high-resolution infrared spectroscopy. *Icarus* **223**, 11–27 (2013). doi:10.1016/j.icarus.2012.11.013

16. V. A. Krasnopolsky, Search for methane and upper limits to ethane and SO_2 on Mars. *Icarus* **217**, 144–152 (2012). doi:10.1016/j.icarus.2011.10.019

17. V. Formisano, S. Atreya, T. Encrenaz, N. Ignatiev, M. Giuranna, Detection of methane in the atmosphere of Mars. *Science* **306**, 1758–1761 (2004). doi:10.1126/science.1101732 Medline

18. A. Geminale, V. Formisano, G. Sindoni, Mapping methane in Martian atmosphere with PFS-MEX data. *Planet. Space Sci.* **59**, 137–148 (2011). doi:10.1016/j.pss.2010.07.011

19. S. Fonti, G. A. Marzo, Mapping the methane on Mars. *Astron. Astrophys.* **512**, A51 (2010). doi:10.1051/0004-6361/200913178

20. S. Fonti, F. Mancarella, G. Liuzzi, T. L. Roush, M. Chizek Frouard, J. Murphy, A. Blanco, Revisiting the identification of methane on Mars using TES data. *Astron. Astrophys.* **581**, A136 (2015). doi:10.1051/0004-6361/201526235

21. C. R. Webster, P. R. Mahaffy, S. K. Atreya, G. J. Flesch, K. A. Farley, MSL Science Team, Low upper limit to methane abundance on Mars. *Science* **342**, 355–357 (2013). doi:10.1126/science.1242902 Medline

22. C. R. Webster, P. R. Mahaffy, S. K. Atreya, G. J. Flesch, M. A. Mischna, P.-Y. Meslin, K. A. Farley, P. G. Conrad, L. E. Christensen, A. A. Pavlov, J. Martín-Torres, M.-P. Zorzano, T. H. McConnochie, T. Owen, J. L. Eigenbrode, D. P. Glavin, A. Steele, C. A. Malespin, P. D. Archer Jr., B. Sutter, P. Coll, C. Freissinet, C. P. McKay, J. E. Moores, S. P. Schwenzer, J. C. Bridges, R. Navarro-Gonzalez, R. Gellert, M. T. Lemmon, MSL Science Team, Mars atmosphere. Mars methane detection and variability at Gale crater. *Science* **347**, 415–417 (2015). doi:10.1126/science.1261713 Medline

23. F. Lefèvre, F. Forget, Observed variations of methane on Mars unexplained by known atmospheric chemistry and physics. *Nature* **460**, 720–723 (2009). doi:10.1038/nature08228 Medline

24. S. K. Atreya, O. Witasse, V. F. Chevrier, F. Forget, P. R. Mahaffy, P. Buford Price, C. R. Webster, R. W. Zurek, Methane on Mars: Current observations, interpretations, and future plans. *Planet. Space Sci.* **59**, 133–136 (2011). doi:10.1016/j.pss.2010.10.008

25. K. J. Zahnle, R. S. Freedman, D. C. Catling, Is there methane on Mars? *Icarus* **212**, 493–503 (2011). doi:10.1016/j.icarus.2010.11.027

26. M. A. Mischna, M. Allen, M. I. Richardson, C. E. Newman, A. D. Toigo, Atmospheric modeling of Mars methane surface releases. *Planet. Space Sci.* **59**, 227–237 (2011). doi:10.1016/j.pss.2010.07.005

27. S. K. Atreya, A.-S. Wong, N. O. Renno, W. M. Farrell, G. T. Delory, D. D. Sentman, S. A. Cummer, J. R. Marshall, S. C. R. Rafkin, D. C. Catling, Oxidant enhancement in martian dust devils and storms: Implications for life and habitability. *Astrobiology* **6**, 439–450 (2006). doi:10.1089/ast.2006.6.439 Medline

28. W. M. Farrell, G. T. Delory, S. K. Atreya, Martian dust storms as a possible sink of atmospheric methane. *J. Geophys. Res.* **33**, L21203 (2006). 10.1029/2006GL027210

29. M. Roos-Serote, S. K. Atreya, C. R. Webster, P. R. Mahaffy, Cometary origin of atmospheric methane variations on Mars unlikely. *J. Geophys. Res.* **121**, 2108–2119 (2016). doi:10.1002/2016JE005076

30. M. Fries, A. Christou, D. Archer, P. Conrad, W. Cooke, J. Eigenbrode, I. L. ten Kate, M. Matney, P. Niles, M. Sykes, A. Steele, A. Treiman, A cometary origin for martian atmospheric methane. *Geochem. Perspect. Lett.* **2**, 10–23 (2016). doi:10.7185/geochemlet.1602

31. P. R. Mahaffy, C. R. Webster, M. Cabane, P. G. Conrad, P. Coll, S. K. Atreya, R. Arvey, M. Barciniak, M. Benna, L. Bleacher, W. B. Brinckerhoff, J. L. Eigenbrode, D. Carignan, M. Cascia, R. A. Chalmers, J. P. Dworkin, T. Errigo, P. Everson, H. Franz, R. Farley, S. Feng, G. Frazier, C. Freissinet, D. P. Glavin, D. N. Harpold, D. Hawk, V. Holmes, C. S. Johnson, A. Jones, P. Jordan, J. Kellogg, J. Lewis, E. Lyness, C. A. Malespin, D. K. Martin, J. Maurer, A. C. McAdam, D. McLennan, T. J. Nolan, M. Noriega, A. A. Pavlov, B. Prats, E. Raaen, O. Sheinman, D. Sheppard, J. Smith, J. C. Stern, F. Tan, M. Trainer, D. W. Ming, R. V. Morris, J. Jones, C. Gundersen, A. Steele, J. Wray, O. Botta, L. A. Leshin, T. Owen, S. Battel, B. M. Jakosky, H. Manning, S. Squyres, R. Navarro-González, C. P. McKay, F. Raulin, R. Sternberg, A. Buch, P. Sorensen, R. Kline-Schoder, D. Coscia, C. Szopa, S. Teinturier, C. Baffes, J. Feldman, G. Flesch, S. Forouhar, R. Garcia, D. Keymeulen, S. Woodward, B. P. Block, K. Arnett, R. Miller, C. Edmonson, S. Gorevan, E. Mumm, The sample analysis at Mars Investigation and instrument suite. *Space Sci. Rev.* **170**, 401–478 (2012). doi:10.1007/s11214-012-9879-z

32. C. R. Webster, P. R. Mahaffy, Determining the local abundance of martian methane and its $^{13}C/^{12}C$ and D/H isotopic ratios for comparison with related gas and soil analysis on the 2011 Mars Science Laboratory (MSL) mission. *Planet. Space Sci.* **59**, 271–283 (2011). doi:10.1016/j.pss.2010.08.021

33. C. R. Webster, P. R. Mahaffy, G. J. Flesch, P. B. Niles, J. H. Jones, L. A. Leshin, S. K. Atreya, J. C. Stern, L. E. Christensen, T. Owen, H. Franz, R. O. Pepin, A. Steele, C. Achilles, C. Agard, J. A. Alves Verdasca, R. Anderson, R. Anderson, D. Archer, C. Armiens-Aparicio, R. Arvidson, E. Atlaskin, A. Aubrey, B. Baker, M. Baker, T. Balic-Zunic, D. Baratoux, J. Baroukh, B. Barraclough, K. Bean, L. Beegle, A. Behar, J. Bell, S. Bender, M. Benna, J. Bentz, G. Berger, J. Berger, D. Berman, D. Bish, D. F. Blake, J. J. Blanco Avalos, D. Blaney, J. Blank, H. Blau, L. Bleacher, E. Boehm, O. Botta, S. Böttcher, T. Boucher, H. Bower, N. Boyd, B. Boynton, E. Breves, J. Bridges, N. Bridges, W. Brinckerhoff, D. Brinza, T. Bristow, C. Brunet, A. Brunner, W. Brunner, A. Buch, M. Bullock, S. Burmeister, M. Cabane, F. Calef, J. Cameron, J. Campbell, B. Cantor, M. Caplinger, J. Caride Rodríguez, M. Carmosino, I. Carrasco Blázquez, A. Charpentier, S. Chipera, D. Choi, B. Clark, S. Clegg, T. Cleghorn, E. Cloutis, G. Cody, P. Coll, P. Conrad, D. Coscia, A. Cousin, D. Cremers, J. Crisp, A. Cros, F. Cucinotta, C. d'Uston, S. Davis, M. Day, M. de la Torre Juarez, L. DeFlores, D. DeLapp, J. DeMarines, D. DesMarais, W. Dietrich, R. Dingler, C. Donny, B. Downs, D. Drake, G. Dromart, A. Dupont, B. Duston, J. Dworkin, M. D. Dyar, L. Edgar, K. Edgett, C. Edwards, L. Edwards, B. Ehlmann, B. Ehresmann, J. Eigenbrode, B. Elliott, H. Elliott, R. Ewing, C.

Fabre, A. Fairén, K. Farley, J. Farmer, C. Fassett, L. Favot, D. Fay, F. Fedosov, J. Feldman, S. Feldman, M. Fisk, M. Fitzgibbon, M. Floyd, L. Flückiger, O. Forni, A. Fraeman, R. Francis, P. François, C. Freissinet, K. L. French, J. Frydenvang, A. Gaboriaud, M. Gailhanou, J. Garvin, O. Gasnault, C. Geffroy, R. Gellert, M. Genzer, D. Glavin, A. Godber, F. Goesmann, W. Goetz, D. Golovin, F. Gómez Gómez, J. Gómez-Elvira, B. Gondet, S. Gordon, S. Gorevan, J. Grant, J. Griffes, D. Grinspoon, J. Grotzinger, P. Guillemot, J. Guo, S. Gupta, S. Guzewich, R. Haberle, D. Halleaux, B. Hallet, V. Hamilton, C. Hardgrove, D. Harker, D. Harpold, A. M. Harri, K. Harshman, D. Hassler, H. Haukka, A. Hayes, K. Herkenhoff, P. Herrera, S. Hettrich, E. Heydari, V. Hipkin, T. Hoehler, J. Hollingsworth, J. Hudgins, W. Huntress, J. Hurowitz, S. Hviid, K. Iagnemma, S. Indyk, G. Israël, R. Jackson, S. Jacob, B. Jakosky, E. Jensen, J. K. Jensen, J. Johnson, M. Johnson, S. Johnstone, A. Jones, J. Joseph, I. Jun, L. Kah, H. Kahanpää, M. Kahre, N. Karpushkina, W. Kasprzak, J. Kauhanen, L. Keely, O. Kemppinen, D. Keymeulen, M. H. Kim, K. Kinch, P. King, L. Kirkland, G. Kocurek, A. Koefoed, J. Köhler, O. Kortmann, A. Kozyrev, J. Krezoski, D. Krysak, R. Kuzmin, J. L. Lacour, V. Lafaille, Y. Langevin, N. Lanza, J. Lasue, S. Le Mouélic, E. M. Lee, Q. M. Lee, D. Lees, M. Lefavor, M. Lemmon, A. Lepinette Malvitte, R. Léveillé, É. Lewin-Carpintier, K. Lewis, S. Li, L. Lipkaman, C. Little, M. Litvak, E. Lorigny, G. Lugmair, A. Lundberg, E. Lyness, M. Madsen, J. Maki, A. Malakhov, C. Malespin, M. Malin, N. Mangold, G. Manhes, H. Manning, G. Marchand, M. Marín Jiménez, C. Martín García, D. Martin, M. Martin, J. Martínez-Frías, J. Martín-Soler, F. J. Martín-Torres, P. Mauchien, S. Maurice, A. McAdam, E. McCartney, T. McConnochie, E. McCullough, I. McEwan, C. McKay, S. McLennan, S. McNair, N. Melikechi, P. Y. Meslin, M. Meyer, A. Mezzacappa, H. Miller, K. Miller, R. Milliken, D. Ming, M. Minitti, M. Mischna, I. Mitrofanov, J. Moersch, M. Mokrousov, A. Molina Jurado, J. Moores, L. Mora-Sotomayor, J. M. Morookian, R. Morris, S. Morrison, R. Mueller-Mellin, J. P. Muller, G. Muñoz Caro, M. Nachon, S. Navarro López, R. Navarro-González, K. Nealson, A. Nefian, T. Nelson, M. Newcombe, C. Newman, H. Newsom, S. Nikiforov, B. Nixon, E. Noe Dobrea, T. Nolan, D. Oehler, A. Ollila, T. Olson, M. Á. de Pablo Hernández, A. Paillet, E. Pallier, M. Palucis, T. Parker, Y. Parot, K. Patel, M. Paton, G. Paulsen, A. Pavlov, B. Pavri, V. Peinado-González, L. Peret, R. Perez, G. Perrett, J. Peterson, C. Pilorget, P. Pinet, J. Pla-García, I. Plante, F. Poitrasson, J. Polkko, R. Popa, L. Posiolova, A. Posner, I. Pradler, B. Prats, V. Prokhorov, S. W. Purdy, E. Raaen, L. Radziemski, S. Rafkin, M. Ramos, E. Rampe, F. Raulin, M. Ravine, G. Reitz, N. Rennó, M. Rice, M. Richardson, F. Robert, K. Robertson, J. A. Rodriguez Manfredi, J. J. Romeral-Planelló, S. Rowland, D. Rubin, M. Saccoccio, A. Salamon, J. Sandoval, A. Sanin, S. A. Sans Fuentes, L. Saper, P. Sarrazin, V. Sautter, H. Savijärvi, J. Schieber, M. Schmidt, W. Schmidt, D. Scholes, M. Schoppers, S. Schröder, S. Schwenzer, E. Sebastian Martinez, A. Sengstacken, R. Shterts, K. Siebach, T. Siili, J. Simmonds, J. B. Sirven, S. Slavney, R. Sletten, M. Smith, P. Sobrón Sánchez, N. Spanovich, J. Spray, S. Squyres, K. Stack, F. Stalport, T. Stein, N. Stewart, S. L. Stipp, K. Stoiber, E. Stolper, B. Sucharski, R. Sullivan, R. Summons, D. Sumner, V. Sun, K. Supulver, B. Sutter, C. Szopa, F. Tan, C. Tate, S. Teinturier, I. ten Kate, P. Thomas, L. Thompson, R. Tokar, M. Toplis, J. Torres Redondo, M. Trainer, A. Treiman, V. Tretyakov, R. Urqui-O'Callaghan, J. Van Beek, T. Van Beek, S. VanBommel, D. Vaniman, A. Varenikov, A. Vasavada, P. Vasconcelos, E. Vicenzi, A. Vostrukhin, M. Voytek, M. Wadhwa, J. Ward, E. Weigle, D. Wellington, F. Westall, R. C. Wiens, M. B.

Wilhelm, A. Williams, J. Williams, R. Williams, R. B. Williams, M. Wilson, R. Wimmer-Schweingruber, M. Wolff, M. Wong, J. Wray, M. Wu, C. Yana, A. Yen, A. Yingst, C. Zeitlin, R. Zimdar, M. P. Zorzano Mier; MSL Science Team, Isotope ratios of H, C, and O in CO_2 and H_2O of the martian atmosphere. *Science* **341**, 260–263 (2013). doi:10.1126/science.1237961 Medline

34. Materials and methods are available as supplementary materials.

35. K. Zahnle, Play it again, SAM. *Science* **347**, 370–371 (2015). doi:10.1126/science.aaa3687 Medline

36. C. E. Newman, J. Gómez-Elvira, M. Marin, S. Navarro, J. Torres, M. I. Richardson, J. M. Battalio, S. D. Guzewich, R. Sullivan, M. Torre, A. R. Vasavada, N. T. Bridges, Winds measured by the Rover Environmental Monitoring Station (REMS) during the Mars Science Laboratory (MSL) rover's Bagnold Dunes Campaign and comparison with numerical modeling using MarsWRF. *Icarus* **291**, 203–231 (2017). doi:10.1016/j.icarus.2016.12.016

37. J. R. C. Garry, I. L. ten Kate, Z. Martins, P. Nørnberg, P. Ehrenfreund, Analysis and survival of amino acids in martian regolith analogs. *Meteorit. Planet. Sci.* **41**, 391–405 (2006). doi:10.1111/j.1945-5100.2006.tb00470.x

38. F. Hourdin, P. Le Van, F. Forget, O. Talagrand, Meteorological variability and the annual surface pressure cycle on Mars. *J. Atmos. Sci.* **50**, 3625–3640 (1993). doi:10.1175/1520-0469(1993)050<3625:MVATAS>2.0.CO;2

39. G. M. Martínez, C. N. Newman, A. De Vicente-Retortillo, E. Fischer, N. O. Renno, M. I. Richardson, A. G. Fairén, M. Genzer, S. D. Guzewich, R. M. Haberle, A.-M. Harri, O. Kemppinen, M. T. Lemmon, M. D. Smith, M. de la Torre-Juárez, A. R. Vasavada, The modern near-surface martian climate: A review of in-situ meteorological data from Viking to Curiosity. *Space Sci. Rev.* **212**, 295–338 (2017). doi:10.1007/s11214-017-0360-x

40. B. M. Jakosky, R. J. Phillips, Mars' volatile and climate history. *Nature* **412**, 237–244 (2001). doi:10.1038/35084184 Medline

41. B. K. Chastain, V. Chevrier, Methane clathrate hydrates as a potential source for martian atmospheric methane. *Planet. Space Sci.* **55**, 1246–1256 (2007). doi:10.1016/j.pss.2007.02.003

42. O. Mousis, J. Simon, J. Bellat, F. Schmidt, S. Bouley, E. Chassefière, V. Sautter, Y. Quesnel, S. Picaud, S. Lectez, Martian zeolites as a source of atmospheric methane. *Icarus* **278**, 1–6 (2016). doi:10.1016/j.icarus.2016.05.035

43. D. Z. Oehler, G. Etiope, *Astrobiology* **17**, 1233–1264 (2017). 10.1089/ast.2017.1657

44. G. Etiope, *Natural Gas Seepage: The Earth's Hydrocarbon Degassing* (Springer, 2015).

45. M. G. Trainer, M. A. Tolbert, C. P. McKay, O. B. Toon, Limits on the trapping of atmospheric CH in martian polar ice analogs. *Icarus* **208**, 192–197 (2010). doi:10.1016/j.icarus.2010.02.006

46. P. R. Pereira, J. Pires, M. Brotas de Carvalho, Adsorption of methane and ethane in zirconium oxide pillared clays. *Separ. Purif. Tech.* **21**, 237–246 (2001). doi:10.1016/S1383-5866(00)00206-9

47. S. Y. Zhang, O. Talu, D. T. Hayhurst, High pressure adsorption of methane in zeolites NaX, MgX, CaX, SrX and BaX. *J. Phys. Chem.* **95**, 1722–1726 (1991). doi:10.1021/j100157a044

48. J. P. Grotzinger, J. Crisp, A. R. Vasavada, R. C. Anderson, C. J. Baker, R. Barry, D. F. Blake, P. Conrad, K. S. Edgett, B. Ferdowski, R. Gellert, J. B. Gilbert, M. Golombek, J. Gómez-Elvira, D. M. Hassler, L. Jandura, M. Litvak, P. Mahaffy, J. Maki, M. Meyer, M. C. Malin, I. Mitrofanov, J. J. Simmonds, D. Vaniman, R. V. Welch, R. C. Wiens, Mars Science Laboratory Mission and Science Investigation. *Space Sci. Rev.* **170**, 5–56 (2012). doi:10.1007/s11214-012-9892-2

49. Curiosity's traverse map through sol 1905; https://mars.nasa.gov/msl/mission/whereistherovernow/?ImageID=9036.

50. J. Gómez-Elvira, C. Armiens, I. Carrasco, M. Genzer, F. Gómez, R. Haberle, V. E. Hamilton, A.-M. Harri, H. Kahanpää, O. Kemppinen, A. Lepinette, J. Martín Soler, J. Martín-Torres, J. Martínez-Frías, M. Mischna, L. Mora, S. Navarro, C. Newman, M. A. de Pablo, V. Peinado, J. Polkko, S. C. R. Rafkin, M. Ramos, N. O. Rennó, M. Richardson, J. A. Rodríguez-Manfredi, J. J. Romeral Planelló, E. Sebastián, M. de la Torre Juárez, J. Torres, R. Urquí, A. R. Vasavada, J. Verdasca, M.-P. Zorzano, Curiosity's Rover Environmental Monitoring Station: Overview of the first 100 sols. *J. Geophys. Res.* **119**, 1680–1688 (2014). doi:10.1002/2013JE004576

51. Á. Vicente-Retortillo, F. Valero, L. Vázquez, G. M. Martínez, A model to calculate solar radiation fluxes on the martian surface. *J. Space Weather Space Clim.* **5**, A33 (2015). doi:10.1051/swsc/2015035

52. M. D. Smith, M.-P. Zorzano, M. Lemmon, J. Martín-Torres, T. Mendaza de Cal, Aerosol optical depth as observed by the Mars Science Laboratory REMS UV photodiodes. *Icarus* **280**, 234–248 (2016). doi:10.1016/j.icarus.2016.07.012

53. Á. Vicente-Retortillo, G. M. Martínez, N. O. Renno, M. T. Lemmon, M. de la Torre-Juárez, Determination of dust aerosol particle size at Gale crater using REMS UVS and Mastcam measurements. *Geophys. Res. Lett.* **44**, 3502–3508 (2017). doi:10.1002/2017GL072589

54. D. M. Hassler, C. Zeitlin, R. F. Wimmer-Schweingruber, S. Böttcher, C. Martin, J. Andrews, E. Böhm, D. E. Brinza, M. A. Bullock, S. Burmeister, B. Ehresmann, M. Epperly, D. Grinspoon, J. Köhler, O. Kortmann, K. Neal, J. Peterson, A. Posner, S. Rafkin, L. Seimetz, K. D. Smith, Y. Tyler, G. Weigle, G. Reitz, F. A. Cucinotta, The Radiation Assessment Detector (RAD) Investigation. *Space Sci. Rev.* **170**, 503–558 (2012). doi:10.1007/s11214-012-9913-1

55. D. M. Hassler *et al*., *Science* **343**, 6169 (2013).

56. J. Guo, C. Zeitlin, R. F. Wimmer-Schweingruber, S. Rafkin, D. M. Hassler, A. Posner, B. Heber, J. Köhler, B. Ehresmann, J. K. Appel, E. Böhm, S. Böttcher, S. Burmeister, D. E. Brinza, H. Lohf, C. Martin, H. Kahanpää, G. Reitz, Modeling the variations of dose rate

measured by RAD during the first MSL martian year: 2012–2014. *Astrophys. J.* **810**, 24–34 (2015). doi:10.1088/0004-637X/810/1/24

57. C. Zeitlin, D. M. Hassler, R. F. Wimmer-Schweingruber, B. Ehresmann, J. Appel, T. Berger, E. Böhm, S. Böttcher, D. E. Brinza, S. Burmeister, J. Guo, J. Köhler, H. Lohf, C. Martin, D. Matthiä, A. Posner, S. Rafkin, G. Reitz, Y. D. Tyler, M. Vincent, G. Weigle, Y. Iwata, H. Kitamura, T. Murakami, Calibration and characterization of the radiation assessment detector (RAD) on Curiosity. *Space Sci. Rev.* **201**, 201–233 (2016). doi:10.1007/s11214-016-0303-y

58. M. G. Trainer *et al*., "Update on the seasonal atmospheric composition measurements by the SAM instrument," abstract 1739, 47th Lunar and Planetary Science Conference (2016).

59. H. B. Franz, M. G. Trainer, C. A. Malespin, P. R. Mahaffy, S. K. Atreya, R. H. Becker, M. Benna, P. G. Conrad, J. L. Eigenbrode, C. Freissinet, H. L. K. Manning, B. D. Prats, E. Raaen, M. H. Wong, Initial SAM calibration gas experiments on Mars: Quadrupole mass spectrometer results and implications. *Planet. Space Sci.* **138**, 44–54 (2017). doi:10.1016/j.pss.2017.01.014

60. http://adsabs.harvard.edu/abs/2011Icar.211.1129M.

61. Mars Rover Curiosity in Artist's Concept, Wide; https://mars.nasa.gov/resources/3512/mars-rover-curiosity-in-artists-concept-wide.

62. P. Sturm, M. Leuenberger, C. Sirignano, R. E. M. Neubert, H. A. J. Meijer, R. Langenfelds, W. A. Brand, Y. Tohjima, Permeation of atmospheric gases through polymer o-rings used in flasks in air sampling. *J. Geophys. Res.* **109** (D4), D04309 (2004). doi:10.1029/2003JD004073